J. Electrochem. Sci. Eng. **15(6)** (2025) 2841; *https://doi.org/10.5599/jese.2841*

Open Access : : ISSN 1847-9286

www.jESE-online.org

Original scientific paper

Electrochemical determination of paracetamol and chlorpheniramine using gold nanoparticles/reduced graphene oxide modified glassy carbon electrode

Huynh Van Chung[1,2], Nguyen Hai Phong[1,✉], Dao Thi Cam Minh[3,✉], Ho Xuan Anh Vu[1], Pham Khac Lieu[1], Nguyen Thi Thanh Huyen[4], Trinh Ngoc Dat[5], Doan Manh Dung[6], Do Thi Duyen[7] and Dinh Quang Khieu[1,✉]

[1]*University of Sciences, Hue University, Hue City, Vietnam*
[2]*Faculty of Pharmacy, Buon Ma Thuot Medical University, Buon Ma Thuot City, Vietnam*
[3]*University of Medicine and Pharmacy, Hue University, Hue City, Vietnam*
[4]*Institute of Research and Development, Duy Tan University, Danang City, Vietnam*
[5]*University of Education and Science, The University of Danang, Danang City, Vietnam*
[6]*Insitute of Biotechnology and Environment, Tay Nguyen University, Buon Ma Thuot, Vietnam*
[7]*Institute of Materials Science, Vietnam Academy of Science and Technology, 18 Hoang Quoc Viet, Cau Giay, Ha Noi city, Vietnam*

Corresponding Authors: ✉*nhphong@hueuni.edu.vn*; ✉*dtcminh@hueuni.edu.vn*; ✉*dqkhieu@hueuni.edu.vn*

Received: June 14, 2025; Revised: August 12, 2025; Published: August 25, 2025

Abstract

One of the significant durability challenges is the corrosion of reinforced concrete. A gold nanoparticle/reduced graphene oxide modified glassy carbon electrode (AuNPs-rGO-GCE) was fabricated using an electrochemical reduction method for the simultaneous determination of paracetamol (PAR) and chlorpheniramine maleate (CPM). AuNPs-rGO modified GC electrodes were prepared through direct electrochemical reduction of GO to rGO, followed by direct reduction of Au ions to Au on the rGO matrix. X-ray diffraction, scanning electron microscopy, Fourier-transform infrared spectra, Raman spectroscopy, energy dispersive X-ray spectroscopy, high-resolution transmission electron microscopy, electrochemical impedance spectroscopy, and X-ray photoelectron spectroscopy characterized the resulting AuNPs-rGO. It was found that AuNPs around 15.4 nm were highly dispersed on the rGO. The modification of GCE by AuNPs-rGO accelerates the electron transfer process and increases the conductivity of the electrode. The AuNPs-rGO modified electrode was used to simultaneously determine PAR and CPM using the square-wave anodic stripping voltammetry (SQW-ASV) method. Under suitable experimental conditions, the SQW-ASV method using AuNPs-rGO-GCE showed a wide linear range from 23.7 to 140.0 µM for PAR and from 7.5 to 54.0 µM for CPM. The limit of detection of PAR and CPM was 7.12 and 2.54 µM, respectively. The proposed SQW-ASV method was applied to analyze PAR and CPM in samples of herbal medicine simultaneously, and the results were compared with those of high-performance liquid chromatography, with no statistical difference.

Keywords
Drug sensors; square-wave anodic stripping voltammetry; electrochemically reduced graphene oxide; herbal medicine

Introduction

Paracetamol (C8H9NO2, PAR), or acetaminophen, is an active ingredient in many pharmaceutical formulations and is widely used due to its analgesic and antipyretic properties. The United Kingdom´s National Health Service proposes a maximum 500 mg dosage every 4 hours for adults [1]. However, paracetamol overdose causes liver and kidney damage [2]. Chlorpheniramine maleate ($C_{16}H_{19}ClN_2{\cdot}C_4H_4O_4$, CPM) is a sedating antihistaminic agent that causes moderate sedation. The most common symptoms are sedation varying from slight drowsiness to deep sleep, dizziness, and gastrointestinal disturbances [3]. A combination of PAR with CPM is introduced to the markets to enhance the therapeutic effect needed in patients with upper respiratory tract infections [4]. Such drugs are usually used against nausea and motion sickness, the common cold, and cough [5]. For this reason, researchers have developed approaches that can be used to simultaneously quantify some or all the active ingredients in a tablet.

Due to its importance, many researchers have focused on analyzing modern and traditional medicines in different forms. Many analytical methods have been developed to simultaneously or separately determine these active ingredients. Chromatographic analytical methods such as reversed-phase high-performance liquid chromatography (RP-HPLC) [6], stationary-phase high-performance thin-layer chromatography (HPTLC) [7], and ultra-high-performance liquid chromatography (UPLC) [8], the HPLC method mainly with UV-Vis detector or photodiode array detector (PAD) or diode array detector (DAD) have been used to simultaneously or separately determine these active ingredients. In addition, the molecular absorption spectroscopy method (UV-Vis) has also been used to determine PAR and CPM [9]. However, the disadvantage of chromatographic analysis, molecular absorption spectroscopy, and capillary electrophoresis is that they often undergo complicated sample treatment stages [9,10]. The voltammetry methods using the electrodes modified by metals and metal oxide nanoparticles and so on, have been recognized as robust approaches for detecting pharmaceutical organic compounds in bioliquids and formulations because they possess key analytical parameters such as high sensitivity, selectivity, low cost, and low detection limits. Nanostructured carbons, metal nanoparticles, and molecularly imprinted polymers modified electrodes were used to determine PAR [11]. A carbon paste electrode modified with ZnO nanoparticles was employed to detect CPM [12]. Samadi et al. conducted simultaneous determination of PAR, phenylephrine hydrochloride, and CPM using nickel phosphate nanoparticles to modify the carbon paste electrode [13]. To the best of our knowledge, few articles have been published to determine PAR and CPM simultaneously using voltammetry methods. In the present paper, an electrochemical sensor based on a reduced graphene oxide/glassy carbon electrode modified by AuNPs (AuNPs-rGO-GCE) was used to simultaneously analyse PAR and CPM by square wave anodic stripping voltammetry (SQW-ASV). This modified electrode showed good reproducibility, repeatability, and accuracy. Experimental results on real samples detected PAR and CPM in some medicines and herbal medicines in Vietnam have been addressed.

Experimental

Materials and reagents

Powder graphite (ϕ < 20 µm, Sigma-Aldrich, USA), sulfuric acid (98 % H_2SO_4, Merck, Germany), phosphoric acid (85 % H_3PO', Merck, Germany), potassium permanganate (99 % $KMnO_4$, Scharlau, Spain), and hydrogen peroxide (30 % H_2O_2, Merck, Germany) were used for material synthesis graphite oxide. Briton-Robinson buffer was prepared from phosphoric acid (85 % H_3PO_4, Merck, Germany), acetic acid (CH_3COOH, Merck, Germany) and boric acid (H_3BO_3, Merck, Germany). The $AuCl_3·HCl$ salts (Sigma-Aldrich, Germany), PAR (100.0 %) and CPM (97.65 %) drugs were purchased from the National Institute of Drug Quality Control of Vietnam (NIDQC). Seven herbal medicines collected from the local area were denoted as BNH093, HCH04, HCH164, VNA01, VNA03, VNA04 and VNA05 for testing PAR and CPM.

Apparatus

Fourier-transform infrared (FT-IR) spectroscopy was performed on an IR Prestige-21, Shimadzu. Raman spectra were performed on a Raman microscopy XPLORATMPLUS, Horiba, Japan, with a diode laser's wavelength of 785 nm. The X-ray diffraction (XRD) patterns were recorded on a D8-ADVANCE (Bruker, Germany). Scanning electron microscopy (SEM) was conducted with a Hitachi S-4800, Japan, and Energy dispersive X-ray spectroscopy (EDX) mapping was performed on a Horiba 7593-H analyser, England. High-resolution transmission electron microscopy (HR-TEM) was recorded on JEM 2100 (Jeol - Japan). Electrochemical impedance spectroscopy (EIS) was conducted on a Metrohm Autolab PGSTAT302 over a frequency range spanning from 100 kHz to 0.01 Hz, the applied DC potential under open-circuit conditions and the amplitude of the AC signal (10 mV). X-ray photoelectron spectra (XPS) were recorded on a Shimadzu Kratos AXISULTRA DLD equipment (Japan), using an X-ray source with an Al target, a generator tube working at 15 kV and 10 mA. Binding energies were calibrated by internal standardization with peak C1s (at 284.6 eV). Peaks were resolved on the Casa XPS software [14].

The electrochemical analysis was performed using a Metrohm 797 instrument (Switzerland) with techniques including cyclic voltammetry (CV) and square-wave anodic stripping voltammetry (SQW--ASV). The electrochemical cell consisted of a three-electrode system in which the working electrode, counter electrode, and reference electrode were a glassy carbon electrode (GCE), a platinum electrode, and Ag|AgCl|3 M KCl, respectively. HPLC comparison measurements of real samples were conducted on a Shimadzu LC-20A series 2000-PAD.

Fabrication of gold nanoparticles/reduced graphene oxide modified glassy carbon electrode

Graphite oxide (GO) was prepared following the literature [15,16]. The GCE was carefully cleaned with 0.03 µm Al_2O_3 powders. Then, it was exposed to a 2 M HNO_3 solution, ethanol, and distilled water several times. Accurately weighed 10 mg of GO was poured into 10 mL of deionized water, and then ultrasonicated for 24 h to obtain the suspension of graphene oxide (GO, 1.0 mg mL^{-1}). Next, a volume of 400 µL of 1 % Nafion, as a binder, was added to 10 mL of GO suspension. Then, 5 µL of the mixture was dropwise dropped onto the polished GCE surface and dried naturally.

The electrochemical reduction of the GO-GCE was conducted by chronoamperometry in 0.1 M PBS, pH 7, at a potential of -1,500 mV and for a time of 120 s to obtain rGO-GCE [17]. The subsequent modification of rGO-GCE with AuNPs to obtain AuNPs-rGO-GCE was conducted using the cyclic voltammetry method with 10 cycles from +500 to -1,000 mV at a rate of 100 mV s^{-1} [18] in the mixture containing 0.01 M H_2SO_4 and 0.2 mM $HAuCl_4$. Bulk samples of reduced graphene oxide (rGO) and

AuNPs materials for physicochemical characterization were synthesized by the electrochemical method under similar experimental conditions. AuNPs-GO materials were prepared using the electrochemical method (AuNPs:GO = 1:10 mass ratio).

Sample preparation

Thong Xoang Tan, a herbal medicine used to treat acute and chronic sinusitis, was selected as a background sample because it was tested and found not to contain any PAR and CPM. The procedure states that m_0 grams of the sample should be weighed accurately into a Falcon tube, after which V_0 mL of 96 % ethanol is to be added. The mixture should then be shaken for 5 minutes, ultrasonicated for 15 minutes, and centrifuged for 10 minutes at 6000 rpm. Following this, it is required that the supernatant be filtered through a 0.45 µm filter to obtain solution A. V_1 mL of solution A is then diluted to V_2 mL using 96 % ethanol to obtain solution B. Solution B is used for analysis. The other samples were prepared using a similar procedure.

Results and discussion

The fabrication of AuNPs-rGO-GCE

GO was first reduced electrochemically using chronoamperometry (Figure 1a). The reduction current changes very rapidly from 0 s to 5 s. Then, it changes slowly from 5 s to 30 s and from 30 s to 120 s; the current intensity changed insignificantly. This result proved the reduction of GO to rGO.

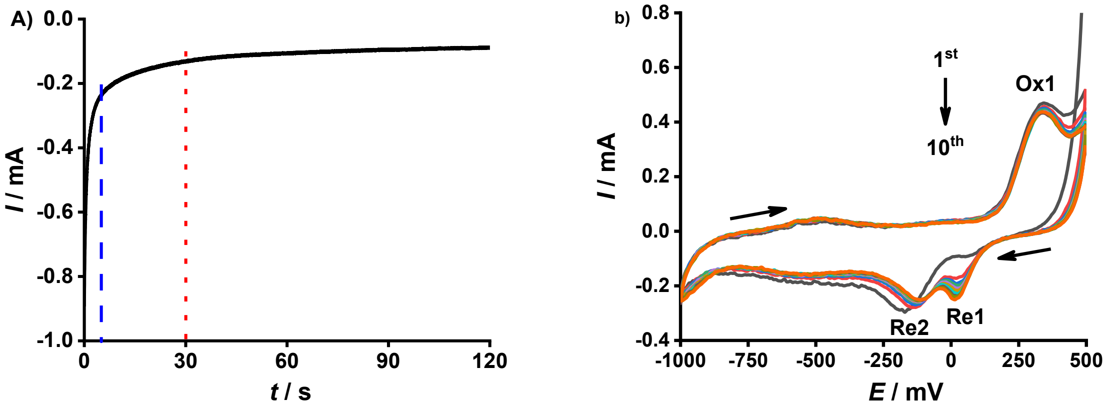

Figure 1. *a) Chronoamperometry curves of GO reduction to rGO (E_{const} = -1,500 mV and t_{meas} = 120 s) and b) cyclic voltammetry curves (CVs) of Au(III) ion reduction to AuNPs on the GCE surface (E_{Begin} = +500 mV, E_{End} = -1,000 mV, ν = 100 mV s^{-1}, CV = 10 cycles, 0.2 mM Au(III) in 0.01 M H_2SO_4)*

Then, electrochemical deposition of gold nanoparticles on rGO-GCE was performed in a cell containing 0.2 mM Au(III) and 0.01 M H_2SO_4 by cyclic voltammetry scanning with a potential starting at +500 mV and ending at -1,000 mV and the number of scans was 10. For the electrochemical synthesis of AuNPs on rGO-GCE, in the first scan (Figure 1b), two reduction peaks appeared at a potential of 79 mV (Re1) can be assigned to due to the Au(III) ion being reduced to Au(I), and -171 mV (Re2) was due to the Au(I) ion being reduced to Au(0), [19]. The Re2 reduction peak is 7.8 times higher than the Re1 reduction peak (see Figure 1b). In the second to tenth scans, the Re1 peak has an irregular change of the peak potential ($E_{P,Re1}$), but the peak current ($I_{P,Re1}$) decreases gradually with each scan. Meanwhile, the Re2 peak has an insignificant change of $E_{P,Re2}$ and $I_{P,Re2}$, with $E_{P,Re2} = -171 \pm 6$ mV, RSD = 5.50 % and $I_{P,Re2} = -0.1520 \pm 0.0060$ mA, RSD = 3.93 % with $n = 9$. This can be explained by the fact that after the first scan, the Au(0) on the electrode surface continues to accumulate and thus increases the current intensity during the oxidation process of Au(0) to Au(I).

Meanwhile, for the oxidation process, only one oxidation peak (Ox1) appeared and did not change much in ten scans, with $E_{P,Ox1}$ = 322 ± 3 mV, RSD: 0.822 %. This may be the oxidation process of Au(0) to Au(III), similar to [18]. But in the 2nd to 10th scans, the Ox1 peak had I_P with almost no change in peak current intensity, with $I_{P,Ox1}$ = 0.201±0.006 mA, RSD = 2.867 %, n = 9. The synthesis of rGO material on the GCE electrode was carried out similarly to the first step of the synthesis of AuNPs-rGO for comparison.

Material characterization

The Fourier transform infrared (FTIR) spectra of the prepared materials are presented in Figure 2a. The vibrations from 3000 to 3600 cm^{-1} are assigned to the ν_{OH} group in the H_2O molecule that is still retained in the materials. The peak at 1718.6 cm^{-1} is characteristic of the ($\nu_{C=O}$) bond in the carbonyl and carboxyl functional groups, but for two materials, AuNPs-GO and AuNPs-rGO, these peaks did not appear, possibly due to overlapping with the vibration of the AuNPs material. The ν_{C-O} bond in the COO- group is ascribed to the vibration at 1392.6 cm^{-1}. The double bond of Csp^2 of GO and rGO is ascribed to the vibration at 1580.0 cm^{-1}. The stretching vibration of the ν_{C-O} bond of the alkoxy group can be shown at two wavelengths of 1076.3 and 1055.1 cm^{-1} [20,21]. Although the peak is not clear, the wave number of 586.4 cm^{-1} for the two AuNPs-GO and AuNPs-rGO materials can show that the AuNPs material is present in the composite material.

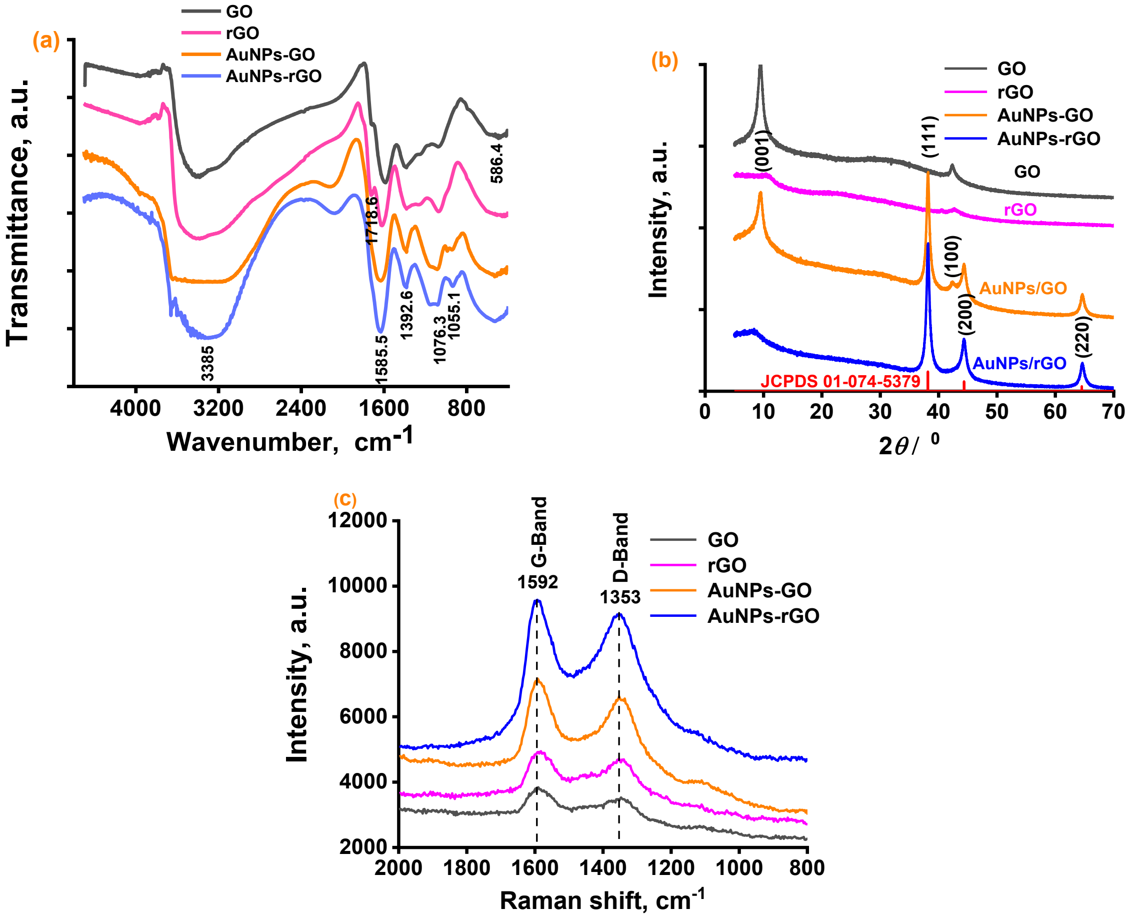

Figure 2. *a) FT-IR spectra, b) XRD patterns, and c) Raman spectra of the prepared materials*

The XRD patterns of the materials are shown in Figure 2b. The GO sample has two distinct peaks at 2θ angles of 9.46 and 42.36°, comparable to the (001) and (100) Miller indices with d-spacings of 9.34 and 2.13 nm. Next, upon electrochemical reduction to reduced graphene oxide (rGO), both peaks showed a significant decrease in intensity and tended to shift to larger diffraction angles because of the functional groups such as hydroxyl, aldehyde, epoxy, and others on the reduced GO [20,21]. This was also observed when the electrochemical reduction of the AuNPs-GO composite material to AuNPs-rGO was carried out; the peak of (100) was almost entirely reduced. On the other hand, for the AuNPs-GO, all the characteristic peaks of (001) and (100) for GO were observed, and three peaks at 38.20, 44.42 and 64.63° with indices (111), (200), and (220) according to JCPDS No.01-074-5379 were assigned to the face-cantered cubic structure of AuNPs [22]. In addition, on the XRD patterns of the AuNPs-GO material, there is still a peak at 44.36°, which may be GO. The three characteristic peaks of AuNPs in AuNPs-rGO still appear quite clearly, but the peaks of the two materials, GO and rGO, decreased very sharply and almost did not appear. This could happen due to the high amplitude of the peaks characteristic of AuNPs overlapping the peaks for rGO [23,24].

The Raman spectra of the samples shown in Figure 2c exhibit two characteristic bands, the D band (~1353 cm^{-1}) and the G band (~1592 cm^{-1}), corresponding to structural defect-induced vibrations (D band) and the vibrations of the sp^2 carbon lattice (G band), respectively. The intensity ratio I_D/I_G is commonly used to evaluate the degree of defects or structural disorder in graphene materials. The obtained I_D/I_G ratios were 0.904 for GO, 0.981 for rGO, 0.8887 for AuNPs-GO, and 0.876 for AuNPs-rGO. The higher I_D/I_G value observed in the rGO sample compared to GO indicates an increase in structural defects after the reduction process, which may be attributed to the formation of discontinuous sp^2 domains as oxygen-containing functional groups are removed. This result shows that the GO material after being electrochemically reduced to rGO has a change in the electronic conjugation state in the structure of GO [25]. This demonstrates the regeneration of the Csp^2-conjugated graphene network after the GO reduction process [24]. Meanwhile, the incorporation of gold nanoparticles (AuNPs) onto the material surface slightly decreased the I_D/I_G ratio in both AuNPs-GO and AuNPs-rGO samples. This suggests that AuNPs may play a role in restructuring or stabilizing the carbon network, thereby reducing the density of defects [26].

The AuNPs-rGO was also studied using the XPS method (Figure 3a-d). The survey XPS spectrum presents C, O, and Au elements as expected (Figure 3d), which suggests that the rGO was decorated with Au nanoclusters. Two distinct doublets for the Au 4f spectra of free Au nanoparticles are introduced in the rGO matrix (Figure 3a), *i.e.* Au $4f_{7/2}$ peak at 83.9 eV and Au $4f_{5/2}$ peak at 87.6 eV. However, concerning the AuNPs-rGO, the Au $4f_{7/2}$ and Au $4f_{5/2}$ peaks at 84.4 and 88.1 eV are consistent with the Au(0) state [27], which has a 0.5 eV red shift compared with that of bulk Au. This shift in binding energy is a typical phenomenon of metal clusters (including Au) on a variety of supporting materials [28]. The C1s spectrum in Figure 3b exhibits five peaks of C-C (284.4 eV), C-O-C (286.7 eV), C=O (287.6 eV), O-C=O/C-O-OH (288.7 eV), which confirm the formation of rGO [29]. In the O 1s spectrum (Figure 3c), the peaks appearing at 531.6, 532.8, and 535.9 eV are attributed to oxygen-containing groups C=O, C-O-H, and H-O-H in rGO, respectively.

The SEM image (Figure 4a) of the material shows a granular surface morphology with diverse particle shapes and sizes. EDX-mapping shown in Figure 4(b-g) reveals the appearances of expected elements, including C, O, and Au. The mass composition of nitrogen in the material accounted for 2.48 %, possibly because of contamination during the synthesis, and Au elements were highly dispersed in the reduced graphene oxide sheets. The HR-TEM image of the AuNPs-rGO material (Figure 4h) shows that the size of the gold particles is distributed very evenly on the rGO matrix and has an average size of 15.6 ± 3.2 nm (Figure 4h, inset).

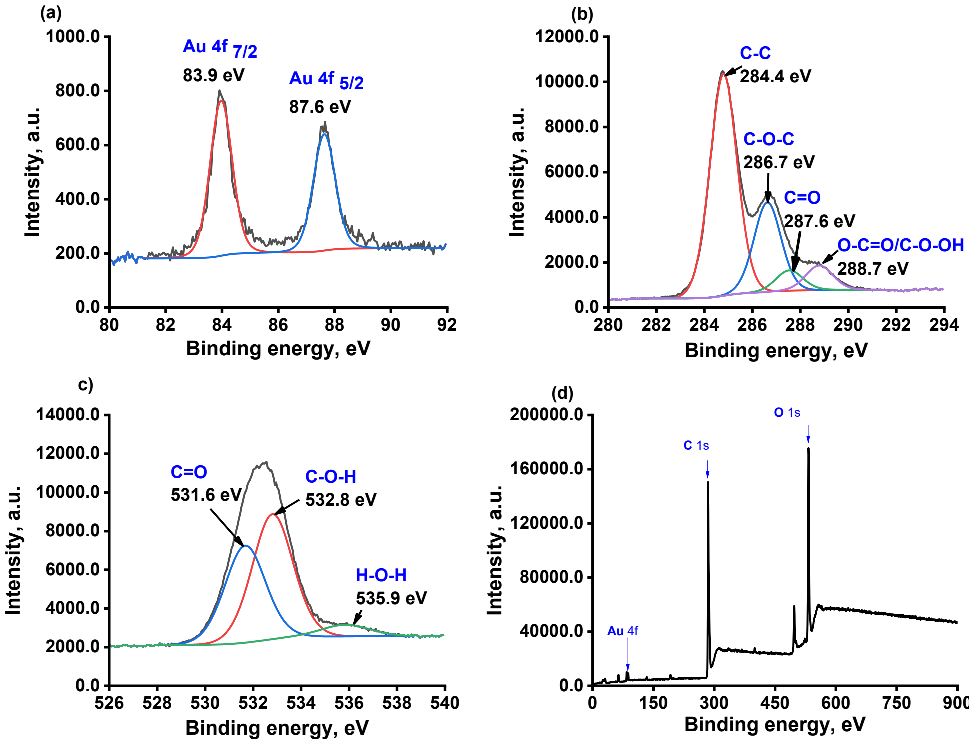

Figure 3. *Narrow scan spectra of: (a) Au 4f, (b) C 1s, (c) O 1s, and (d) XPS survey spectrum of AuNPs-rGO*

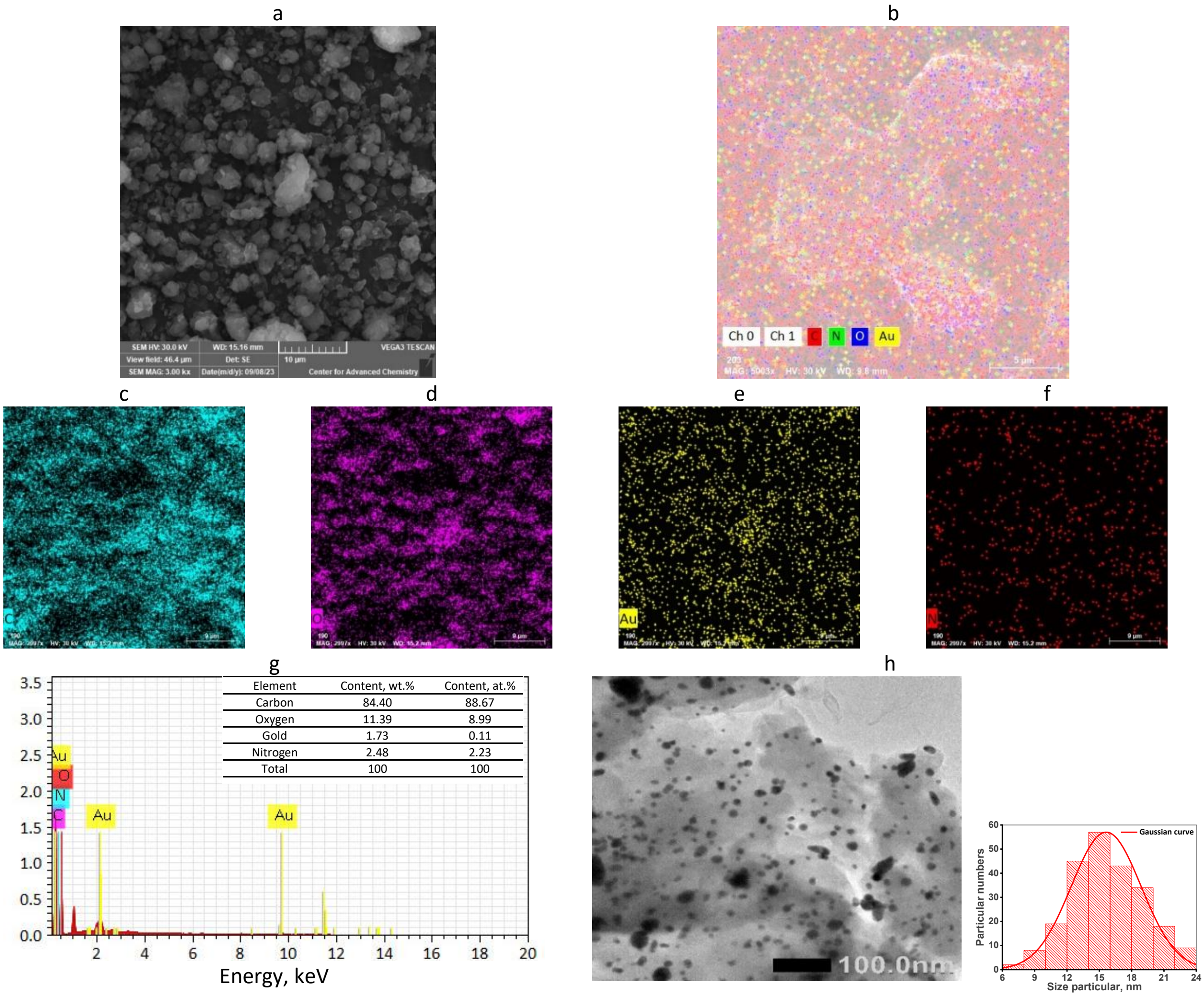

Element	Content, wt.%	Content, at.%
Carbon	84.40	88.67
Oxygen	11.39	8.99
Gold	1.73	0.11
Nitrogen	2.48	2.23
Total	100	100

Figure 4. *(a) SEM image, (b) composite mapping, (c) carbon, (d) oxygen, (e) gold, (f) nitrogen, (g) EDX spectrum, and (h) HR-TEM image of AuNPs-rGO (the inset presents particle size distribution counted for 250 particles)*

Electrochemical behaviour

In electrochemical methods, the peak current intensity (I_P) depends on many factors, including the electrochemically active surface area and the total impedance of the working electrode. The surface area of the working electrode is determined by the Randles-Ševčik equation for the reversible system [30,31] and CVs in Figure 5a. The average electrochemically active surface area for GCE, GO-GCE, rGO-GCE, AuNPs-GO-GCE and AuNPs-rGO-GCE were 0.0358±0.0002, 0.0173±0.0007, 0.0431±0.0020, 0.0475±0.0005 and 0.0574±0.0015 cm^2, respectively. Notably, the electroactive surface areas of AuNPs-rGO-GCE modified electrode were 1.21, 1.33, 3.32 and 1.60 times higher than the AuNPs-GO-GCE, rGO-GCE, GO-GCE and GCE electrodes, respectively.

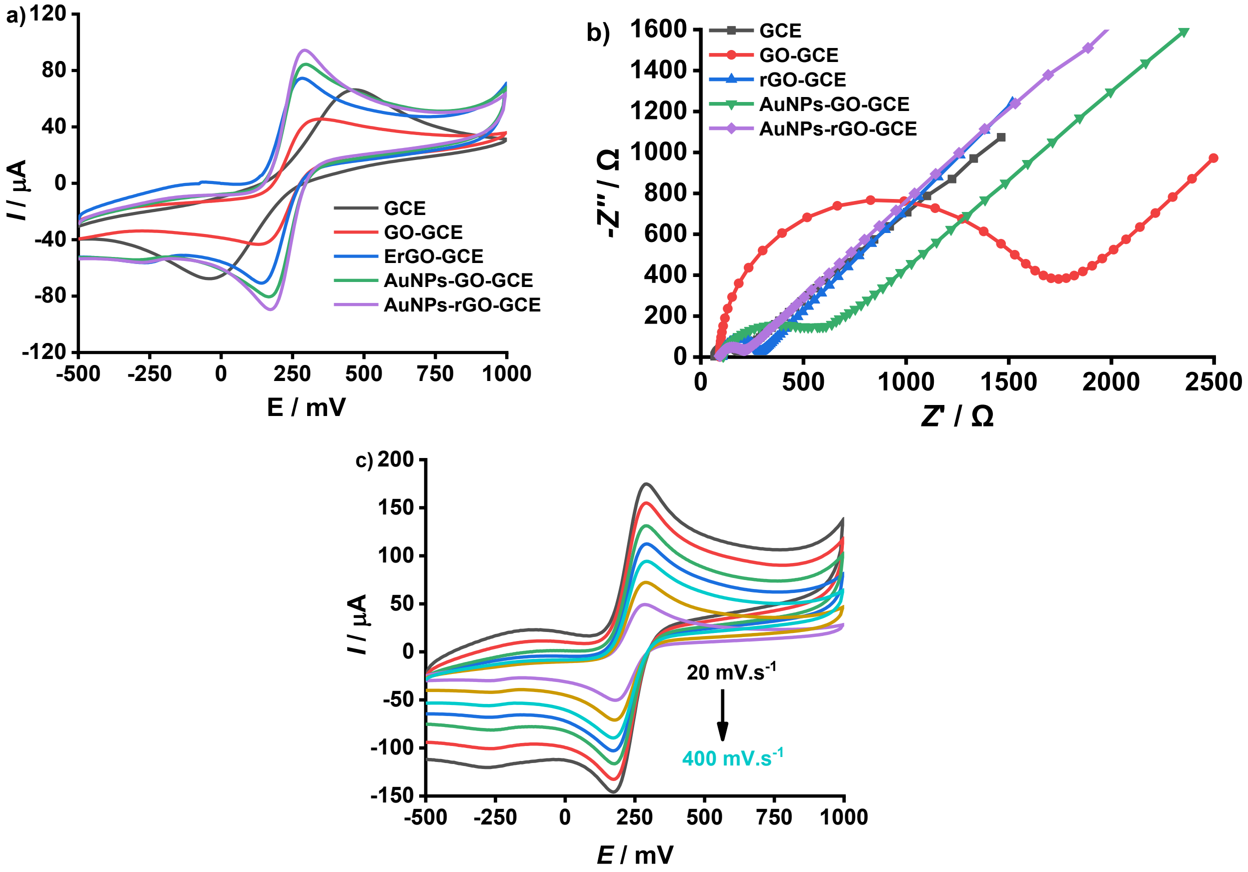

Figure 5. *(a) CV curves (100 mV s^{-1}) and (b) Nyquist plots of base and modified GC electrodes in 0.1 M KCl with 5 mM [Fe(CN)$_6$/Fe(CN)$_6$]$^{3-/4-}$, (c) CV curves at different potential scan rates (20 mV s^{-1} to 400 mV s^{-1})*

The electrochemical impedance of the working electrode could help to characterize the charge transfer process and evaluate charge transfer resistance (R_{ct}) values of the base and modified electrode types (Figure 5b). R_{ct} values were calculated through the diameter of a semicircle at higher frequencies, for the bare GCE, GO, AuNPs-GO and AuNPs-rGO-GCEs in KCl solution containing [Fe(CN)$_6$/Fe(CN)$_6$]$^{3-/4-}$ redox pair. The obtained R_{ct} values were 109.8, 1537.4, 170.8, 527.3 and 122.3 Ω. Compared to GO material, the R_{ct} values of two modified materials, rGO and AuNPs-rGO, were significantly reduced by 9.0 and 12.6 times, respectively. This result demonstrated the reconstruction of the Csp^2 configuration in the rGO sheet, indicating that electrical conductivity improved after the electrochemical reduction process. The AuNPs-rGO-GCE had the smallest value of R_{ct} (122.3 Ω) and the most significant area (0.0574 cm^2), suggesting an accelerated electron transfer process and increased conductivity of the electrode.

On the other hand, for the AuNPs-rGO-GCE electrode, Figure 5c shows that the anodic peak potential (E_{AP}) does not change. Meanwhile, the cathodic peak potential (E_{CP}) does not change much, with RSD of 3.726 % after seven potential scans from 20 mV s^{-1} to 400 mV s^{-1}. E_{PA} = 292±000 mV, RSD = 0.000 % (n = 7); E_{CP} = 172 ± 6 (mV), RSD = 3.726 % (n = 7). Although ΔE_P ($|E_{PA} - E_{PC}|$) = 120 mV is not equal to the theoretical value of 59 mV [30], the I_{AP}/I_{CP} ratio at seven different potential scan rates from 20 to 400 mV s^{-1} was approximately equal to unity, with the I_{AP}/I_{CP} ratio: 0.98 ± 0.02 and RSD = 1.852 % indicating that the electrochemical currents for the redox reactions on the AuNPs-rGO-GCE surface were well-matched, and the system exhibited quasi-reversible behaviour.

CV curves of PAR and CPM responses at four types of modified GC electrodes are shown in Figure 6a. Figure 6b shows that the role of rGO material is very suitable in the stage of analyte accumulation, such as PAR and CPM [32,33], compared to GO material. In addition, the combination of rGO and AuNPs materials increased the I_P of PAR and CPM (Figure 6b). Therefore, the AuNPs-rGO-GCE modified electrode was used in this study.

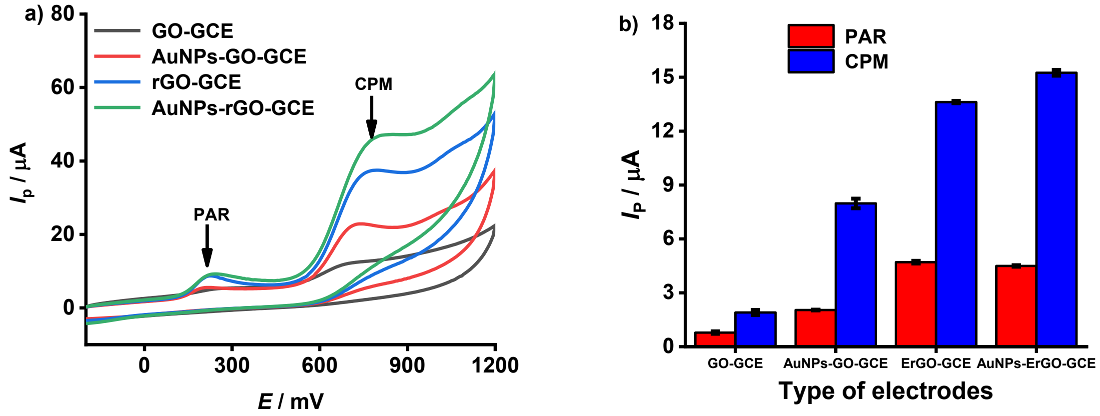

Figure 6. *a) CV curves (100 mV s^{-1}) and b) I_P variations of PAR and CPM at different modified GC electrodes in 0.05 M BR buffer, pH 7, C_{PAR} = 70 µM, C_{CPM} = 54 µM, E_{acc} = -500 mV, t_{acc} = 60 s*

Effect of graphene oxide volume and pH on AuNPS/rGO-GCE response

The amount of nanocomposite material was investigated based on a 1.0 mg mL^{-1} GO suspension, which was drop-cast onto the surface of a glassy carbon electrode (GCE) and electrochemically reduced to form a rGO film. The volume of AuNPs-rGO suspension significantly affects the electroactive surface area, the film thickness, and the conductivity of the working electrode, thereby influencing the peak current response of PAR and CPM, as well as the sensitivity in both CV and SQW-ASV methods. As the suspension volume increased from 2 to 8 µL, the peak currents (I_p) of PAR and CPM gradually increased and reached their maximum values at 6 µL for PAR and 5 µL for CPM (Figure 7a and 7b). The initial increase in volume enhanced the electroactive surface area and the number of catalytic sites, thereby improving sensitivity. However, when the volume exceeded 6 µL, the resulting GO film became too thick, hindering the efficient electrochemical reduction of GO to rGO and reducing electron transfer efficiency. Conversely, a volume below 5 µL was insufficient to fully cover the electrode surface with active material, resulting in a smaller electroactive area and fewer catalytic sites, leading to a lower current response. Notably, within the optimal range of 5 to 6 µL, the I_p values for PAR showed minimal variation in real sample applications, indicating good stability and reproducibility of the modified electrode.

The volume of 5.0 µL is the volume that many studies have proposed for dropping on the surface of GC electrodes with diameters from 2.8 to 3 mm, which is very convenient [34,35]. Therefore, the volume of GO of 5.0 µL (1.0 mg mL^{-1}) is found suitable for further studies.

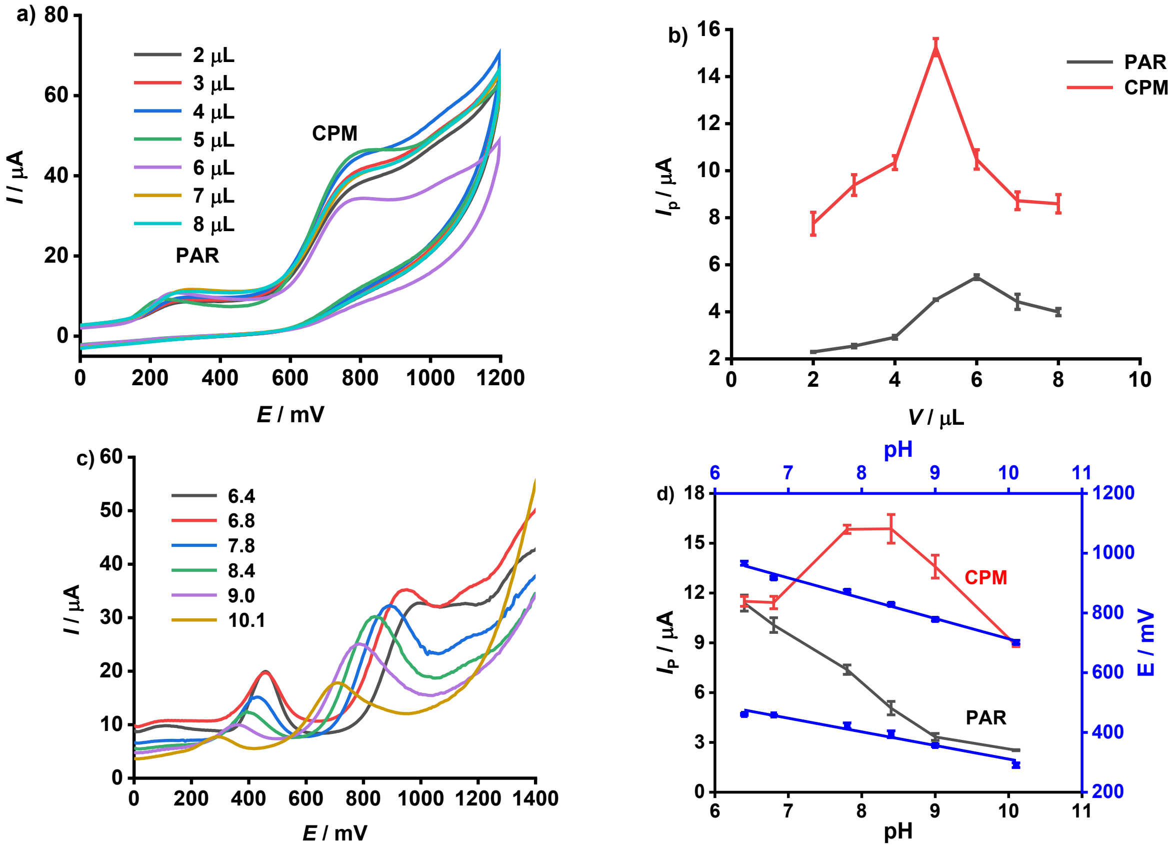

Figure 7. *a) CVs (100 mV s^{-1}) of AuNPS/rGO-GCE with different GO volumes (1.0 mg mL^{-1}) in 0.05 M BR buffer, pH 7, C_{PAR} = 70 µM, C_{CPM} = 54 µM, E_{acc} = -500 mV, t_{acc} = 60 s and b) I_P of PAR and CPM in dependence on GO volume. c) SQW-ASV curves (ΔE = 25 mV, f = 20 Hz, U_{Step} = 6 mV) of PAR and CPM at different pH and d) I_P and E_p of PAR and CPM in dependence on pH*

In this study, the SQW-ASV method was used to investigate the effect of pH on the stripping signal of PAR and CPM. The electrochemical response of both PAR and CPM is strongly influenced by the pH of the supporting electrolyte, which affects the protonation/deprotonation states of the analytes. The oxidation potential and peak current are closely related to the compounds' pK_a values. For PAR (pK_a ≈ 9.38), the oxidation involves a proton-coupled electron transfer mechanism, which becomes more favourable in its deprotonated form at higher pH values. Similarly, CPM (pK_a ≈ 9.2) exhibits enhanced electrochemical activity when it transforms from its protonated to neutral or deprotonated state, facilitating electron transfer at the electrode surface. The pH effect on the electrochemical signals was investigated from pH 6.4 to 10.1 using Britton-Robinson buffer (Figure 7c). As shown in Figure 7d, the I_P of PAR decreased sharply as pH increased, whereas the I_P of CPM tended to increase and reached a maximum at pH 7.8. Meanwhile, the I_P of PAR is still large enough at 7.383±0.2835 µA, n = 4. Therefore, the pH value of 7.8 was considered acceptable for determining PAR and CPM in subsequent studies. On the other hand, the E_P of PAR and CPM shifted toward the negative side as the pH increased. This confirmed that H$^+$ ions participate in the electrochemical reaction of PAR and CPM [35,36]. In addition, there is a linear correlation between E_P and pH, described with Equations (1) and (2) (Figure 7d):

$$E_{PAR} = (830 \pm 65) - (53 \pm 8)\ \text{pH},\ R^2 = 0.9884 \tag{1}$$

$$E_{CPM} = (1{,}402 \pm 70) - (69 \pm 9)\ \text{pH},\ R^2 = 0.9929 \tag{2}$$

It was found that the slopes of Equations (1) and (2) are close to the theoretical value of 59 mV pH^{-1} according to the Nernst equation. Therefore, an equal number of electrons and protons is involved in the oxidation of PAR and CPM at the modified electrode. When considering the mechanism of the electrochemical reaction of PAR, various studies using different modified electrodes have reported the number of electrons and protons exchanged during the oxidation process. The general consensus is that two electrons and two protons are exchanged as shown in Scheme 1.

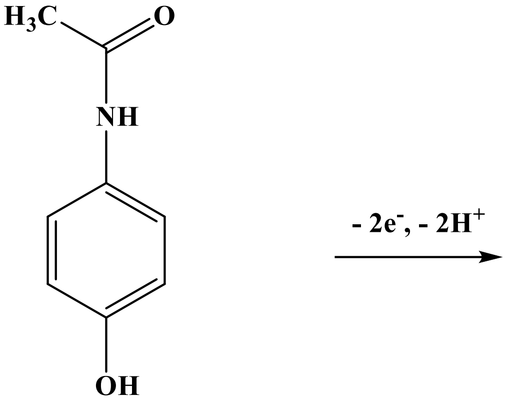

Scheme 1. *The mechanism of PAR oxidation*

For CPM, there are very few research works, where authors have different and inconsistent discussions. Therefore, in this paper, some changes are proposed: i) the number of protons exchanged is determined to be equal to (≈ 1), but when the electrochemical reaction mechanism is proposed, it gives one product [37]. On the other hand, according to [36,38], it gives two products; ii) although in the proposed mechanism, two electrons and two protons are exchanged, in the overall reaction, there is only one [34,39,40]; iii) according to [41] and [42], it is assumed that CPM exchanges two electrons and protons. In addition, the overall reaction gives two products, 3-(4-chlorophenyl)-3-(pyridine-2-yl) propanal and dimethylamine. Therefore, based on the information that the molecular structure of CPM contains a saturated tertiary amine and two unpaired electrons, this is the centre of the electrochemical reaction. In addition, the intermediate product is a quaternary amine Schiff base, which is very unstable and will be hydrolysed. Therefore, we propose the electrochemical reaction mechanism of CPM as presented in Scheme 2.

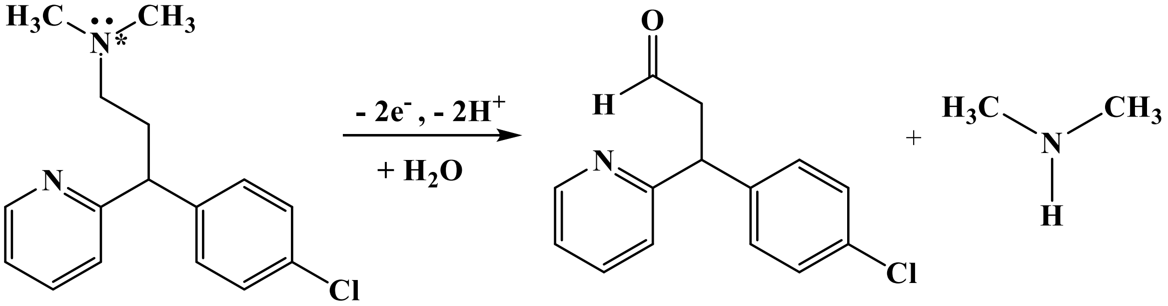

Scheme 2. *The proposed mechanism of CPM oxidation*

Scan rate effect

The scan rate effect on the electrochemical signals of PAR and CPM at AuNPs-rGO-GCE is presented in Figure 8a. From the figure, it is evident that this is an irreversible system because only anodic peak appears, but no cathodic peak appears. The linear relationship between peak current (I_p) and the square root of scan rate ($\nu^{1/2}$) could provide kinetic information. The line with a non-zero intercept suggests this is an adsorption-controlled process; otherwise, this is a process controlled by diffusion. From Equations (3) and (4), the 95 % confidence interval of the intercept did not contain zero, indicating that the intercepts of the two linear regression equations of CPM and

PAR did not pass through the origin. This suggests that the adsorption process prevails at the modified electrode, based on the Randles-Ševčik equation for the irreversible system [30,31,43].

$$I_{\mathrm{P,PAR}} = (1.689 \pm 0.815) + (0.217 \pm 0.061)\, v^{1/2},\ R^2 = 0.9606 \tag{3}$$

$$I_{\mathrm{P,CPM}} = (8.870 \pm 1.264) + (0.485 \pm 0.095)\, v^{1/2},\ R^2 = 0.9806 \tag{4}$$

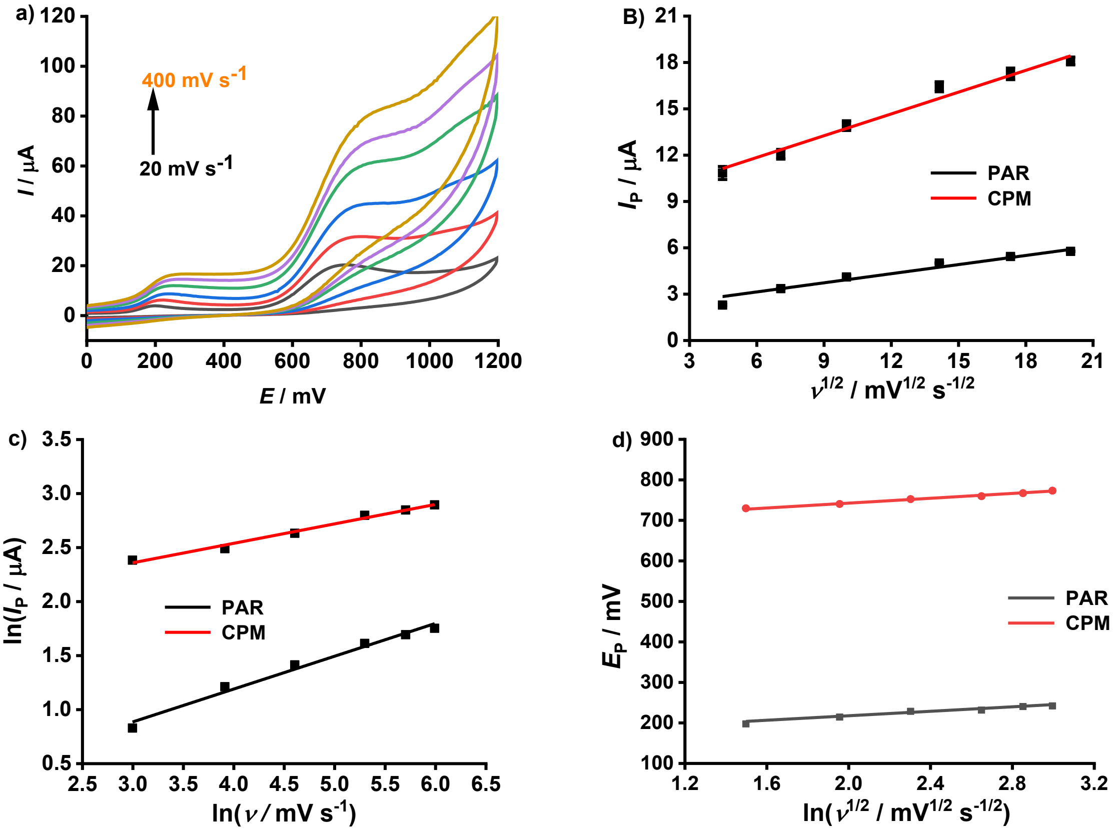

Figure 8. *(a) Cyclic voltammetry curves of PAR and CPM on AuNPs-rGO-GCE at different potential scan rates; (b) regression curves between I_P and $\nu^{1/2}$ of PAR and CPM; (c) ln I_P vs. ln ν plots, (d) E_P vs. ln $\nu^{1/2}$ plots (E_{acc} = -500 mV, t_{acc} = 60 s, scan rate varied from 20 to 400 mV s^{-1}, C_{PAR} = 70 µM, C_{PM} = 54 µM, BR buffer 0.05 M, pH 7)*

The relationship between ln I_P and ln ν (Figure 8c) provides the concentration of PAR and CPM per unit electrochemically active area of the modified electrode [30,38,44]. The surface coverage (Γ) was calculated using Equation (5):

$$\ln I_p = \ln\left(\frac{n^2F^2A\Gamma}{4RT}\right) + \ln \nu \tag{5}$$

which can come to the expression presented by Equation (6)

$$\Gamma = \frac{e^a\, 4RT}{n^2\, F^2 A} \tag{6}$$

where a represents the y-intercept of the linear regression line describing the logarithmic relationship between peak current intensity (ln I_p) and scan rate (ln ν), n is the number of transferred electrons, R is the gas constant (8.314 J mol^{-1} K^{-1}), T = 298 K is the temperature in Kelvin, F is the Faraday constant (96,500 C mol^{-1}), A is the electrochemically active surface area [44].

Through the slopes of the two Equations (7) and (8) based on Figure 8c, the values of surface coverage were calculated as Γ_{PAR}: 4.753×10^{-6} mol cm^{-2} and Γ_{CPM}: 5.549×10^{-6} mol cm^{-2}, respectively.

$$\ln I_{\mathrm{P,PAR}} = (-0.025 \pm 0.262) + (0.304 \pm 0.054) \ln \nu,\quad R^2 = 0.9840 \tag{7}$$

$$\ln I_{\mathrm{P,CPM}} = (1.820 \pm 0.137) + (0.180 \pm 0.028) \ln \nu,\quad R^2 = 0.9874 \tag{8}$$

Therefore, the adsorbed quantity accumulated of PAR and CPM on the modified electrode surface was quite large in 60 seconds, similar to Shetti *et al.* [39]. When compared to the Rajpurohit *et al.* [37] using electrodes modified with manganese hexacyanoferrate/chitosan (MnHCF/CS) material, the Γ_{CPM} was much larger, 13,400 times.

The kinetics of the electrochemical reaction were also studied by examining the effect of the potential scan rate on the stripping signal [43,45]. The electron transfer coefficient (α) was calculated using the equation $\alpha = RT/bnF$, where b is the slope of linear plots from the correlation between E_{P} and ln $\nu^{1/2}$. From the slope of linear plots in Figure 8d, and the correlation between E_{P} and ln $\nu^{1/2}$ defined by Equations (9) and (10), the electron transfer coefficient (α) of PAR and CPM was determined to be α_{PAR} = 0.434 and α_{CPM} = 0.449. Both values are approximately 0.5, which is in complete agreement with the theory for irreversible systems [31,43].

$$E_{\mathrm{P,PAR}} = (154 \pm 9) + (30 \pm 4) \ln \nu^{1/2},\ R^2 = 0.9923 \tag{9}$$

$$E_{\mathrm{P,CPM}} = (686 \pm 8) + (29 \pm 3) \ln \nu^{1/2},\ R^2 = 0.9930. \tag{10}$$

Optimizing the operational parameters of the anodic stripping voltammetry square-wave method

The operational parameters, including accumulation potential (E_{acc}), accumulation time (t_{acc}), square wave frequency (f), pulse amplitude (ΔE), and potential step (U_{step}), were optimized. As shown in Figure S1, when the E_{acc} varied from -1,200 to -900 mV, the peak potential (E_{P}) changed insignificantly. This showed that the external potential applied to the working electrode was not related to the electrochemical reaction on the AuNPs-rGO-GCE. When the potential was shifted from 1,200 mV to -900 mV, the I_{P} of PAR did not differ much, but for CPM there was a very significant increase and reached a maximum at the E_{acc} of -900 mV. When E_{acc} shifted to a more positive direction to -400 mV, the I_{P} of PAR and CPM both decreased sharply, although still far from the PAR stripping peak. The subsequent experiments shifted to -100 mV, and the I_{P} of PAR and CPM also did not change (not shown here). To determine PAR and CPM simultaneously, the E_{acc} of -900 mV was chosen.

Figure S2 shows that when the t_{acc} increased from 5 to 30 s, the I_{P} raised gradually. When the t_{acc} was greater than 30 seconds, the I_{P} of PAR showed minimal change, but the I_{P} of CPM still increased, possibly due to the adsorption process of PAR and CPM being almost saturated on the surface of the modified electrode. To reduce the analysis time, t_{acc} = 30 s was found appropriate.

The results of the square wave frequency survey from 5 to 50 Hz corresponding to the potential sweep rate from 30 to 300 mV s^{-1} are shown in Figure S3. When the square wave frequency fluctuates from 5 to 15 Hz, the I_{P} of PAR and CPM both increased sharply, but from 20 to 50 Hz, *i.e*. with the potential sweep rate from 120 to 300 mV s^{-1}, there was a slow increase. Since the square wave frequency was related to the potential sweep rate, and therefore, the frequency of 20 Hz with a potential scanning rate of 120 mV s^{-1} was appropriate. ΔE is a parameter that significantly affects the electrochemical signals of the analyte in the SQW-ASV method. When the pulse amplitude is small, the stripping peak current will be small and when the pulse amplitude is large, the stripping peak current will be large, but this leads to an increase in the full width at half maximum (FWHM). Therefore, it affects the selectivity of the analytical method. The results in Figure S4 show that the E_{P} of PAR and CPM did not change significantly when the pulse amplitude varied from 5 to 60 mV. Meanwhile, the I_{P} of CPM increased quite linearly, but for PAR, it increased linearly from 5 to 30 mV with a large slope and then increased slowly. On the other hand, when increasing the pulse amplitude from 5 to 60 mV, the FWHM varied from 95 to 161 mV with PAR and from 156 to 183 mV, which was quite large. Therefore, increasing the pulse amplitude increased the I_{P}, but reduced the selectivity and the I_{P} can easily fall out of the linear range. Therefore, the pulse amplitude of 30 mV is considered appropriate.

Limit of detection and linear range

The aim is to simultaneously analyse PAR and CPM in aqueous solutions and apply them to some pharmaceutical samples. The study was conducted for three cases: *i*) the first case was to fix the CPM concentration at 54 µM and gradually increase the PAR concentration from 7 to 700 µM, *ii*) the second case was to fix the PAR concentration at 28 µM and progressively increase the CPM concentration from 10.8 to 194.4 µM, and *iii*) the third case was to add PAR and CPM simultaneously, with PAR from 7.0 to 280 µM and CPM from 10.8 to 70.2 µM.

In the case of fixing the concentration of CPM, the I_P of PAR gradually increased from 7.0 to 360 µM, but from 360 µM it increased very slowly to 588 µM, where it increased almost insignificantly (Figure 9a).

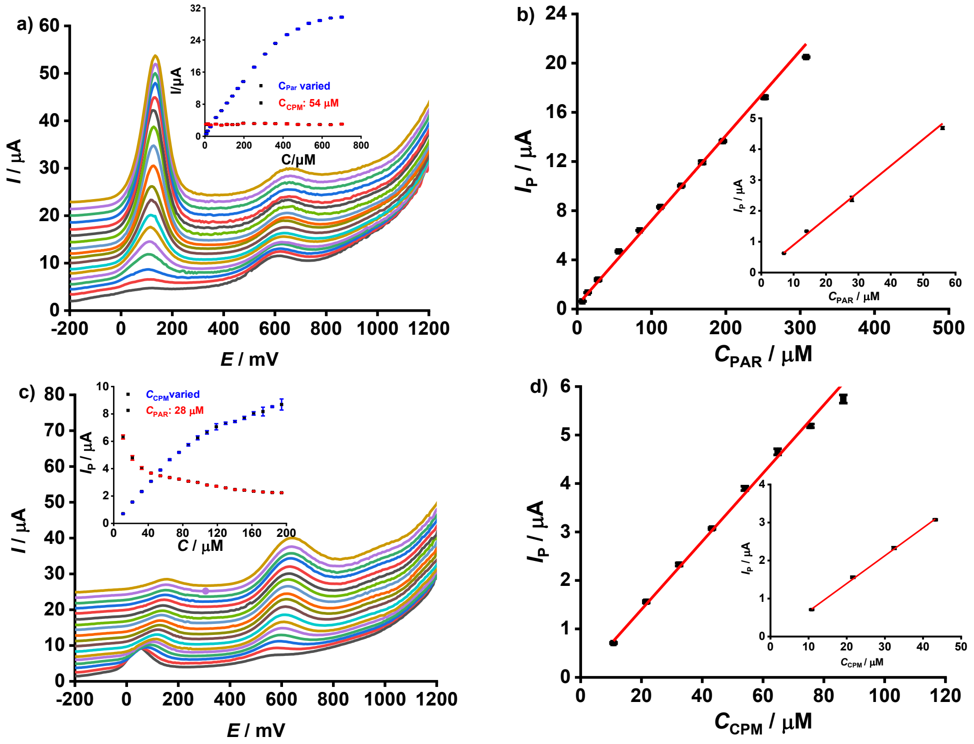

Figure 9. *(a) SQW-ASV curves of AuNPs-rGO-GCE at constant CPM concentration of 54 µM, and PAR concentrations varied from 7 to 700 µM; (b) calibration plot of I_p versus concentrations of PAR from 7.0 to 308 µM; inset: used for LOD determination with PAR concentrations from 7.0 to 56 µM; (c) SQW-ASV curves of AuNPs-rGO-GCE at constant PAR concentration of 28 µM, and CPM concentrations varied from 10.8 to 194 µM; d) calibration plot of I_p* vs. *concentration of CPM from 10.8 to 86.4 µM; inset: used for LOD determination with CPM concentrations from 10.8 to 43.2 µM* (E_{acc}=-900 mV, t_{acc}=30 s, ΔE=30 mV, U_{Step}=6 mV, f=20 Hz, ν=120 mV s^{-1}, BR buffer 0.05 M, pH 7)

Meanwhile, the I_P of CPM did not change significantly with $I_{P,CPM}$ = 3.046±0.149 µA, *n* = 18 and RSD = 4.903 % and therefore, compared to ½ RSD_H at 54 µM concentration (5.33 %) was acceptable [46]. On the other hand, $E_{P,CPM}$ and $E_{P,PAR}$ did not change much, with $E_{P,CPM}$ = 616±14 mV, *n* = 18 and $E_{P,PAR}$ = 115±10 mV, *n* = 18. This shows that 54 µM CPM did not affect the determination of PAR.

According to [47], the determination of LOD usually chooses the concentration range near the origin and therefore, the concentration range was selected from 7.0 to 56 µM (the inset of Figure 9b). The results are presented by Equation (11):

$$I_{P,PAR} = (0.114 \pm 0.268) + (0.082 \pm 0.008)\, C_{PAR},\ R^2 = 0.9989 \tag{11}$$

The calculated LOD_{PAR} = 2.65 µM and LOQ_{PAR} = 8.85 µM completely satisfy conditions: 10×LOD>C_{min} and LOD<C_{min}, LOQ = 3.33×LOD [47,48]. Thus, the linear range in the fixed 54 µM CPM field of PAR is from 8.85 µM to 308 µM.

In the second case, when the concentration of PAR is fixed at 28.0 µM, the I_P of CPM gradually increased from 10.8 to 194.4 µM. However, the increase of I_P could be divided into two distinct stages: from 10.8 to 97.2 µM (9th addition), it increases rapidly, and from 97.2 to 194.4 µM, it increases slowly. However, at the concentration of CPM of 54.0 µM (5th addition), nearly twice the concentration of PAR, the I_P of PAR decreases very sharply. Next, increasing the concentration of CPM to 194.4 µM, the I_P of PAR still tended to decrease slowly (Figure 9c). Thus, when the concentration of CPM was doubled, it had a significant effect on the stripping signal of PAR. In addition, $E_{P,PAR}$ shifted towards the positive direction quite clearly (Figure 9c) from the 5th addition. But from the 6th to the 18th addition, the shift was slow, with $E_{P,PAR}$ = 134±15 mV, n = 13 and RSD = 10.9 %. Meanwhile, $E_{P,CPM}$ almost changed insignificantly, with $E_{P,CPM}$ = 603 ± 23 mV, n = 18 and RSD = 3.83 %. Thus, in terms of electrochemical and chemical reactions, since $E_{P,\ CPM}$ did not change and $I_{P,\ CPM}$ still increased linearly from 10.8 to 97.2 µM, it is assumed that CPM did not interact with PAR. The decrease in $I_{P,CPM}$ may be due to the fact that CPM molecules have larger spatial structures, so they competitively adsorb with PAR onto the surface of the AuNPs-rGO-GCE during the accumulation stage. Similar to the consideration for PAR alone, LOD and LOQ were determined, while fixing the PAR concentration at 28 µM and the CPM concentration from 10.8 to 43.2 µM, *i.e.* the concentration range close to the origin, giving the following results, Equation (12):

$$I_{P,CPM} = (-0.047 \pm 0.209) + (0.073 \pm 0.007)\ C_{CPM}\ ,\ R^2 = 0.9990 \tag{12}$$

giving LOD_{CPM} = 1.63 µM and LOQ_{CPM} = 5.44 µM.

The calculated LOD fully satisfies conditions of 10×LOD>C_{min} and LOD<C_{min}, LOQ = 3.33 LOD.

After determining the LOD and LOQ, the working concentration range of CPM at the fixed PAR concentration of 28 µM is from 10.8 to 97.2 µM and the linear range is from 5.44 to 86.4 µM.

Finally, the simultaneous addition of PAR and CPM with specific concentration ranges was conducted, with PAR concentration changing from 7.0 to 280 µM and CPM from 10.8 to 70.2 µM. The results obtained after 12 additions, and each measurement repeated three times, are presented in Figure 10a. In Figure 10b, it was found that the linear range of PAR and CPM has narrowed at high concentrations compared to the cases of examining each PAR and CPM compound individually. As a result, with PAR: from 7.0 to 140 µM and with CPM: from 10.8 to 54.0 µM. This is reasonable because when adding PAR and CPM simultaneously, during the accumulation stage, the adsorption process will be almost saturated on the surface of the modified electrode. At the same time, it is also possible that due to competitive adsorption, the I_P of PAR and CPM may decrease compared to the individual examination. As a result, the sensitivity decreases, leading to an increase in the detection limit. From the studied concentration ranges of PAR and CPM, linear regression Equations (13) and (14) were constructed as follows (Fig. 10c and 10d):

$$I_{P,PAR} = (0.599 \pm 0.791) + (0.090 \pm 0.025)\ C_{PAR},\ R^2 = 0.9921 \tag{13}$$

$$I_{P,CPM} = (0.321 \pm 0.542) + (0.090 \pm 0.027)\ C_{CPM},\ R^2 = 0.9902 \tag{14}$$

As reported in previous studies [47,48], LOD and LOQ for PAR and CPM were determined using linear regression data points near the origin, in accordance with the 3σ criterion. The inset plots in Figures 10(a) and 10(b) were utilized for these calculations. Based on this approach, the calculated values were LOD_{PAR} = 7.122 µM and LOQ_{PAR} = 23.740 µM, whereas LOD_{CPM} = 2.544 µM and LOQ_{CPM} = 8.480 µM.

Here, the obtained results on the linear ranges and detection limits for PAR and CPM at AuNPs-rGO-GCE are compatible with those obtained at different electrodes and already published in the literature, as shown in Table 1.

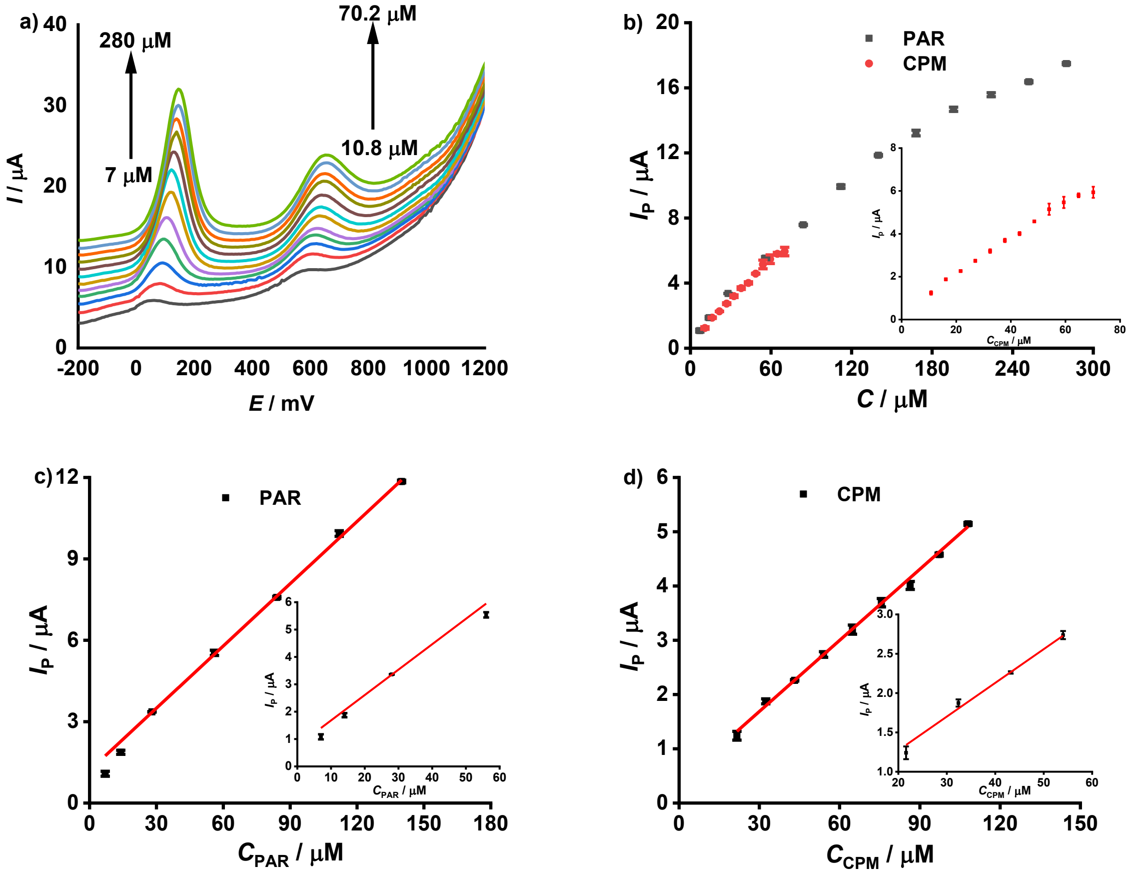

Figure 10*. (a) SQW-ASV curves of AuNPs-rGO-GCE for PAR (7 to 280 μM) and CPM (10.8 to 70.2 μM); (b) variation of I_p for PAR and CPM at different spiked concentrations; (c) calibration plot of I_p versus PAR concentration (7 to 140 μM), inset: LOD determination (7 to 56 μM); (d) calibration plot of I_p versus CPM concentration (10.8 to 54 μM), inset: LOD determination (10.8 to 27 μM).* (E_{acc} *-900 mV,* t_{acc} *30 s,* ΔE*=30 mV,* U_{Step}*=6 mV,* f*=20 Hz,* ν*=120 mV* s^{-1}*, BR buffer 0.05 M, pH 7)*

Table 1. *A comparison of analytical performance of CPM and PAR at different electrodes taken from the literature, and AuNPs-rGO-GCE from the present work*

Electrode	Method, pH	Linear range, μM	LOD, μM	Sample	Ref.
G-NS/GCE	DPV, pH 7.3	10 - 60	0.062	Serum and urine	[34]
IL/CNT/GCE	LSV, pH 7.0	1.0 - 900	0.7	Tablet	[35]
CPE	DPV, pH 9.2	8.0 - 100	1.7	Tablet and serum	[42]
AuNP-p(L-met)/PGE	DPV, pH 4.0	CPM: 9.74 - 718 PAR: 3.18 - 3000	CPM: 2.92 PAR: 0.95	Pharmaceuticals and serum	[49]
MWCNTs-IL/GCE	DPV, pH 12.0	1.4 - 99.7	0.40	Pharmaceuticals	[50]
MWCNT/GCE	DPV, pH 10.0	5 - 500	1.63	Serum	[51]
Au@Ag/p-L-met/PGE	DPV, pH 7.0	0.87 - 600.0	0.26	Pharmaceuticals	[38]
rGO/AgNPs/GCE	SWV, pH 10.0	10 - 300	4.2	Pharmaceuticals and artificial urine	[40]
Ni-NPs/CPE	DPV, pH 7.0	CPM: 50 - 10000 PAR: 750 - 7000	CPM: 16 PAR: 140	Tablet	[13]
Ru/Pty/GCE	DPV, pH 10.1	2.0 - 45	0.338	Tablet and siro	[52]
AuNPs-rGO-GCE	SWV, pH 7.5	CPM: 8.480 - 54 PAR: 23.74 - 140	CPM: 2.54 PAR: 7.12	Herbal medicine	This study

Abbreviations: DPV: Differential pulse voltammetry; SWV: Square wave voltammetry; CPE: Carbon paste electrode; GCE: Glassy carbon electrode; PGE: Pencil graphite electrode NiP NPs: Nickel phosphate nanoparticles; Ru/Pty: tris(2,2’-bipyridyl)Ru(II) and Pty: polytyramine; MWCNT: Multiwalled carbon nanotubes; AuNP-p(L-met): Gold nanoparticles-poly (L-methionine); G-NS: Graphene nanosheet; p-L-met: poly(L-methionine).

Repeatability and reproducibility

Experiments were conducted with four different concentrations of PAR and CPM to evaluate the repeatability of the stripping signal in Figure 11. The repeatability evaluation was based on the statistical quantity of relative standard deviation (RSD, %) [48,53]. The experimental I_P and RSD values were compared with the 1/2 RSD_H to 2/3 RSD_H values of the Howitz function (RSD_H) [46] and according to AOAC [54] at different concentrations of PAR and CPM. The results showed that the experimental relative standard deviation ($\text{RSD}_\text{Ex.}$) values at all concentrations of PAR and CPM were much smaller than ½ RSD_H. As cited in [54], the allowable RSD values in the concentration range from 10 to 100 *ppm* are 7.3 and 5.3 %. Thus, the repeatability of I_P for PAR and CPM is considered acceptable.

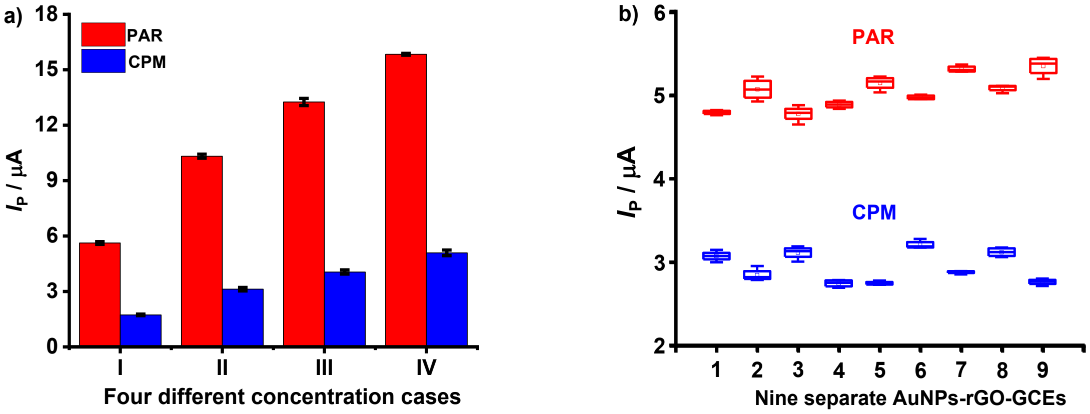

Figure 11. *(a)* I_p *of SQW-ASV curves of AuNPs-rGO-GCE with PAR and CPM at different concentration pairs with nine replicate measurements: (I)* C_{PAR} *= 56 µM and* C_{CPM} *= 32.4 µM; (II)* C_{PAR} *= 126 µM and* C_{CPM} *= 64.8 µM; (III)* C_{PAR} *= 168 µM and* C_{CPM} *= 86.4 µM; (IV)* C_{PAR} *= 224 µM and* C_{CPM} *= 108 µM; (b)* I_P *variation of PAR and CPM at nine AuNPs-rGO-GCEs fabricated by the same procedure,* $C_{PAR} = C_{CPM}$ *= 28 µM.* (E_{acc} *-900 mV,* t_{acc} *30 s,* ΔE*=30 mV,* U_{Step}*=6 mV, f=20 Hz,* ν*=120 mV* s^{-1}*, BR buffer 0.05 M, pH 7)*

The reproducibility of the proposed method was assessed by measuring the electrochemical signals at different electrodes modified using the same procedure (Figure 11b). The modification process was repeated 9 times to give 9 separate AuNPs-rGO-GCEs. The results showed that the E_P of PAR and CPM had an irregular shift. This result was not due to the chemical interaction between PAR and CPM but could be due to the change in potential of the reference electrode Ag/AgCl|3 M KCl, or it could also be due to the modification for each time not being uniform. As seen in Figure 11b, the I_P of PAR and CPM changed almost insignificantly, with I_p for PAR being 5.043±0.206 µA (n = 9), RSD = 4.092 %, and i_p for CPM being 2.942±0.185 µA (n = 9), RSD = 6.277 %. At the concentrations of PAR (4.232 ppm) and CPM (7.694 ppm), when compared with 2/3 RSD_H [46,48], the deviations were minor, specifically with PAR, RSD_H = 8.587 % and with CPM, RSD_H = 7.847 %. On the other hand, compared with AOAC [54], it was also smaller than the predicted standard deviation of 8 % at an analyte concentration of 1 ppm. In addition, when studying the linear range, it was still shown that the I_P of PAR and CPM increased linearly with the concentration of the standard spiking. In summary, the reproducibility of the AuNPs-rGO-GCE modified electrode for simultaneous analysis of PAR and CPM is found acceptable.

Effect of interfering substances

The selected interfering substances include three groups: *i*) salts of metals commonly found in the environment, such as $Al(NO_3)_3$, $Ca(NO_3)_2$, $FeCl_3$, K_2HPO_4, $Mg(NO_3)_2$, and NaCl; *ii*) toxic metals such as $Cd(NO_3)_2$, $CuCl_2$, $Cd(NO_3)_2$ and $ZnSO_4$. These two groups of metals were surveyed at concentrations 20 to 100 times higher; *iii*) organic compounds present in pharmaceuticals and biochemical environments such as caffeine (CAF), D-glucose (D-Glu), propylene glycol (PG), sorbitol (SOB), uric acid (UA), and ascorbic acid (AA). For organic substances, AA, UA, and CAF were surveyed at concentrations from 2 to 10 times higher; the remaining substances were from 20 to 100 times higher. The concentrations of PAR and CPM were fixed at 28 µM, *i.e.* C_{PAR} = 4.233 ppm and C_{CPM} = 7.694 ppm. The effects of interfering substances are shown in Figure 12.

Among 16 compounds studied, AA, UA, and CAF had peaks in the voltammetry curves ranging from -200 to +1200 mV (Figure S5). In particular, with UA (twice the concentration), there was a phenomenon of overlapping peaks with the peak of PAR, and when AA was present in the solution, the E_{P} of PAR and CPM was shifted to the positive side. Thus, with concentrations 4 to 10 times higher than AA, UA, and CAF, it was impossible to quantify PAR and CPM because of the $\mathrm{RSD_{Ex}}$. was larger from 1/2 $\mathrm{RSD_H}$ to 2/3 $\mathrm{RSD_H}$ [46,54]. Organic substances, D-Glu, PG, and SOB did not affect the stripping signals of PAR and CPM.

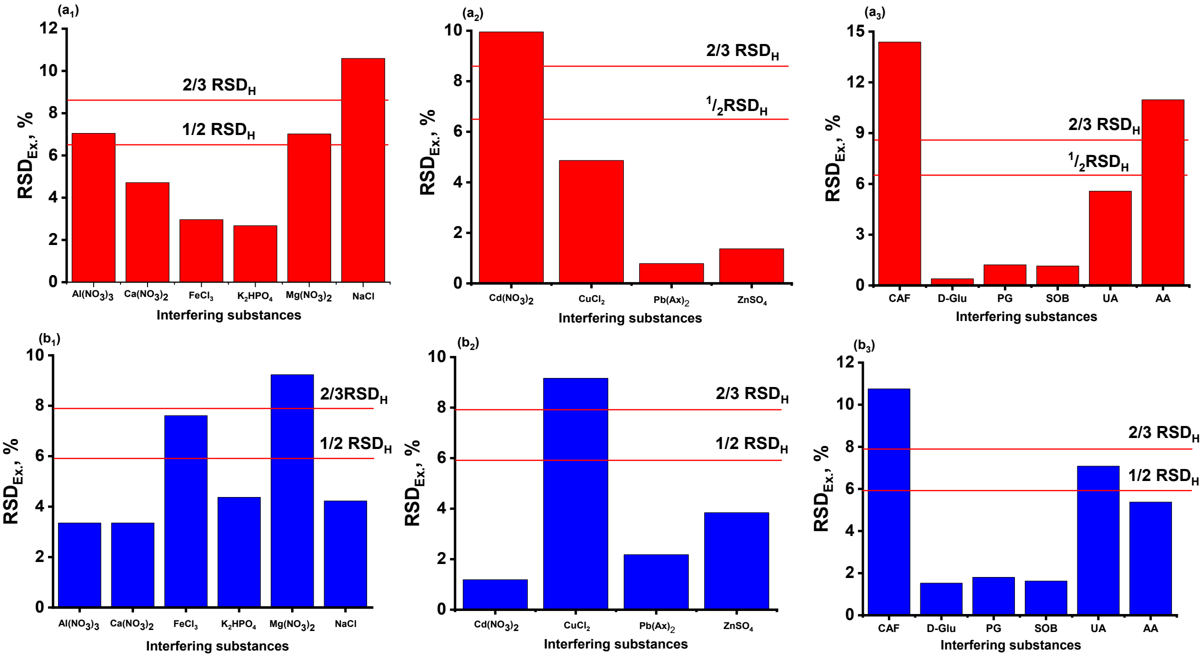

Figure 12. *Relative standard deviations ($\mathrm{RSD_{Ex.}}$), n = 4 of $I_{\mathrm{P,PAR}}$ (a_1, a_2, a_3) and $I_{\mathrm{P,CPM}}$ (b_1, b_2, b_3) on AuNPs-rGO-GCE after adding 16 different inorganic and organic interfering species (E_{acc} -900 mV, t_{acc} 30 s, ΔE=30 mV, U_{step}=6 mV, f=20 Hz, ν=120 mV s^{-1}, C_{PAR}=C_{CPM}=28 µM, BR buffer 0.05 M, pH 7)*

Inorganic compounds like NaCl and $Cd(NO_3)_2$ had $\mathrm{RSD_{Ex}}$ values less than 2/3 $\mathrm{RSD_H}$ of the I_{P} signal of PAR, so they did not affect the electrochemical signals. In addition, $Mg(NO_3)_2$ and $CuCl_2$ salts significantly affect the I_{P} of CPM. Meanwhile, all other metal salts do not affect the stripping signal of PAR and CPM. In addition, no dissolution peaks of all metals appear on the stripping voltammetry curves (Figure S6).

Recovery and real sample analysis

The real samples used were two formulations: *i*) the first sample has PAR in the composition but no CPM (denoted TD1), *ii*) the second sample has CPM in the composition but no PAR (denoted TD2), and *iii*) the third sample is a herbal medicine sample that does not have two components PAR and CPM, meaning the sample is negative (denoted DT3). Samples were prepared as described in sample preparation. The accuracy of the SQW-ASV method using AuNPs-rGO-GCE was determined through the recovery value (Rev) at three concentration levels of a standard addition to the initial solution (Table 2).

Table 2*. Results of determining the accuracy of the SQW-ASV method*

TD1 (PAR)				TD2 (CPM)			
Concentration[a], mg mL^{-1}			Rev, %	Concentration[a], mg mL^{-1}			Rev, %
PAR	Added	Found		CPM	Added	Found	
77.27	239.0	328.0	104.9	435.3	212.0	644.0	98.47
	424.0	517.0	103.7		668.4	1076	95.86
	742.0	820.0	100.1		1018	1460	100.7
DT3							
PAR				CPM			
Concentration[a], mg mL^{-1}			Rev, %	Concentration[a], mg mL^{-1}			Rev, %
PAR	Added	Found		CPM	Added	Found	
0	444.0	463.1	104.3	0	274.4	281.2	102.5
	742.0	739.7	99.70		848.0	882.1	104.0
	1484	1509	101.72		1384	1331	96.15

[a]The concentrations are converted to the volume of the solution after standardization (V_2 / mL as used in sample preparation)

The recovery values in two pharmaceutical samples ranged from 95.86 to 104.9 %, and one herbal medicine ranged from 96.15 to 104.3 % for all three concentrations spiked into the original samples. This result is entirely satisfactory compared to AOAC [54], and therefore, the method's accuracy is acceptable.

The selected herbal medicines were prepared before the simultaneous determination of PAR and CPM by two methods: SQW-ASV using AuNPs-rGO-GCE and the HPLC method.

Table 3 shows the herbal medicine samples containing two components, PAR and CPM, and the herbal medicine samples containing only CPM.

Table 3*. Contents of PAR and CPM in herbal medicine samples with two components*

Sample	m_0 / g	Analyte	Found content, mg g^{-1}		Relative error, %
			SQW-ASV[a]	HPLC-DAD	
BNH093	0.3321	PAR	198.2 ± 2.648	197.2	-0.471
		CPM	16.46 ± 0.6660	16.74	-1.032
HCH04	0.4705	PAR	141.5 ± 0.6660	141.0	+0.384
		CPM	0.757 ± 0.4340	0.792	-4.361
HCH164	0.3876	PAR	34.00 ± 1.759	34.17	-0.505
		CPM	0.478 ± 0.2160	0.461	+3.676
VNA01	0.3357	CPM	5.764 ± 2.046	5.831	-1.15
VNA03	0.2874	CPM	6.761 ± 2.046	6.952	-2.75
VNA04	0.2824	CPM	7.300 ± 1.754	7.573	-3.60
VNA05	0.3643	CPM	2.118 ± 2.046	2.146	-1.33

[a]The mean value $x_{TB} \pm t_{Crit.}(p = 0.05, n = 3) \times U_y$. The combined uncertainty of y is calculated as:

$U_y = \sqrt{\sum_{i=1}^{n} U_{xi}}$ where U_y and U_{xi} were uncertainty of content and values [47]

On the other hand, relative error is considered a statistical quantity used to evaluate the accuracy of the analytical method [55] as well as to compare the results of two different analytical methods [56]. Thus, relative error values range from -4.361 to +3.676 % for 7 herbal medicine samples containing one and two components of PAR and CPM (Table 3), indicating the differences between the two methods were acceptable. Statistical comparison using paired sample t-test showed that there was no significant difference between the two methods ($t(4) = 0.824$, $p = 0.228 > 0.05$) for PAR; $t(4) = -1.830$, $p = 0.07 > 0.05$) for CPM. These results indicate the proposed method is accurate. The results of simultaneous analysis of PAR and CPM in real samples by the proposed method are shown in Table 3, showing that the mixing of PAR and CPM in foods has been banned in the production and trading of health protection foods, but still exists [57]. On the other hand, by referring to some published documents, some countries such as China, Korea and Iran have also found the mixing of PAR and/or CPM in herbal medicines [58-60].

Conclusions

The electrochemical sensor based on an AuNPs-rGO-modified glassy carbon electrode (GCE) demonstrated effective simultaneous detection of paracetamol (PAR) and chlorpheniramine maleate (CPM). The electrode was fabricated *via* a simple, rapid, low-cost, and environmentally friendly electrochemical method. Structural and morphological analyses confirmed the uniform distribution of gold nanoparticles on the rGO surface, which enhanced electrical conductivity and facilitated electron transfer. The SQW-ASV technique using the AuNPs-rGO-GCE exhibited high sensitivity, low detection limits, and high precision, with acceptable recovery. Moreover, the proposed method was successfully applied to the simultaneous quantification of PAR and CPM in herbal medicine samples. The results showed no statistically significant difference compared to those obtained by the HPLC-DAD method, confirming the reliability and accuracy of the electrochemical approach. These findings highlight the practical potential of AuNPs-rGO-based electrochemical sensors for pharmaceutical analysis.

Supplementary material: *Additional data are available electronically on article page of the journal's website: https://pub.iapchem.org/ojs/index.php/JESE/article/view/2841, or from the corresponding author upon request.*

Author contributions: *H.V.C and N.H.P conceived of the conceptualization. H.V.C and D.T.C.M contributed to the study draft, and formal analysis; D.T.C.M contributed to funding acquisition; H.X.A.V, P.K.L, T.N.D and N.T.T.H performed investigation and methodology; D.T.D and D.M.D conducted the validation. D.Q.K. and N.H.P conducted writing - original draft, and writing -review& editing. All authors provided critical feedback and approved the final manuscript.*

Funding: *This research was funded by the Ministry of Education and Training (VN) under project code B2023-DHH-10.*

Conflict of interest*: The authors declare no competing interests.*

Data availability: *All data that supports the findings of this study is available in the published article and/or the Supplementary material of this article.*

Ethics declaration*: not applicable*

References

[1] National Health Service, *Paracetamol for adults*, 2018, https://www.nhs.uk/medicines/paracetamol-for-adults/. (date accessed: May 18, 2024)

[2] D. N. Bateman, J. W. Dear, H. K. Thanacoody, S. H. Thomas, M. Eddleston, E. A. Sandilands, J. Coyle, J. G. Cooper, A. Rodriguez, I. Butcher, S. C. Lewis, A. D. Vliegenthart, A. Veiraiah, D. J. Webb, A. Gray, Reduction of adverse effects from intravenous acetylcysteine treatment for paracetamol poisoning: a randomised controlled trial, *Lancet* **383** (2014) 697-704. https://doi.org/10.1016/s0140-6736(13)62062-0

[3] Ç. Tas, Y. Özkan, A. Savaser, T. Baykara, In vitro release studies of chlorpheniramine maleate from gels prepared by different cellulose derivatives, *Il Farmaco* **58** (2003) 605-611. https://doi.org/10.1016/S0014-827X(03)00080-6

[4] S. Y. Yang, J. S. Byun, J. H. Hwang, J. J. An, K. E. Hong, W. Kang, Y. K. Lee, Y. . Park, Study of Instruments for Assessment and Clinical Research Trends in Common Cold, *The Journal of Korean Medicine* **29** (2008) 165-181 https://koreascience.kr/article/JAKO200817963246474.pdf

[5] S. S. Nitin Borkar, Review of Simultaneous determination of analytes by High Performance Liquid Chromatography (HLPC) in multicomponent cough and cold oral drug products., *International Journal of PharmTech Research* **3** (2011) 1339-1345 https://www.researchgate.net/publication/266370935

[6] M. F. H. Al-Samarrai, M. Z. Lafta, M. J. T. Al-Abbasee, O.J. Muhammad, Development and Validation of a RP-HPLC Method for Simultaneous Quantification of Paracetamol and Phenylephrine Hydrochloride, *International Journal of Design & Nature and Ecodynamics* **19** (2024) 275-280. https://doi.org/10.18280/ijdne.190130

[7] A. Arage, T. Layloff, A. Hymete, A. Ashenef, High performance thin layer chromatography (HPTLC) method development and validation for the simultaneous determination of paracetamol, caffeine, chlorpheniramine and phenylepherine in tablet formulation, *Acta Chromatographica* **35** (2023) 170-178. https://doi.org/10.1556/1326.2022.01028

[8] M. A. Mohamed, Stability-Indicating New RP-UPLC Method for Simultaneous Determination of a Quaternary Mixture of Paracetamol, Pseudoephedrine, Chlorpheniramine, and Sodium Benzoate in (Cold–Flu) Syrup Dosage Form, *Journal of AOAC International* **105** (2022) 703-716. https://doi.org/10.1093/jaoacint/qsac002

[9] L. C. D. Chawe, N. K. Tittikpina, S. M. Ndiaye, B. N. Amadou Diop, D. Fall, Y. M. Diop, S. O. Sarr, Validation of an UV-Visible spectrophotometry assay method for the determination of chlorpheniramine maleate tablets without prior extraction, *International Journal of Biological and Chemical Sciences* **15** (2021) 273-281. https://doi.org/10.4314/ijbcs.v15i1.24

[10] United States Pharmacopeia and National Formulary, *USP 43 – NF 38*, Rockville, MD: United States Pharmacopeial Convention, USA, 2020. http://182.160.97.198:8080/xmlui/handle/123456789/1493

[11] M. Stoytcheva, Z. Velkova, V. Gochev, B. Valdez, M. Curiel, Advances in electrochemical sensors for paracetamol detection: Electrode materials, modifications, and analytical applications, *International Journal of Electrochemical Science* **20** (2025) 100924. https://doi.org/10.1016/j.ijoes.2024.100924

[12] H. asadollahzadeh, Developing an electrochemical sensor based on a carbon paste electrode modified with ZnO nanoparticles synthesized by microwave for determination of chlorpheniramine maleate, *Analytical Methods in Enviromental Chemistry Journal* **4** (2021) 16-25. https://doi.org/10.24200/amecj.v4.i01.130

[13] A. Samadi-Maybodi, S. K. Hassaninejad-Darzi, H. Nejad-Darzi, H. Ilkhani, A New Sensor for Determination of Paracetamol, Phenylephrine Hydrochloride and Chlorpheniramine Maleate in Pharmaceutical Samples Using Nickel Phosphate Nanoparticles Modified Carbon Past Electrode, *Analytical and Bioanalytical Electrochemistry* **3** (2011) 134-145 https://www.researchgate.net/publication/234166408

[14] N. Fairley, V. Fernandez, M. Richard-Plouet, C. Guillot-Deudon, J. Walton, E. Smith, D. Flahaut, M. Greiner, M. Biesinger, S. Tougaard, D. Morgan, J. Baltrusaitis, Systematic and collaborative approach to problem solving using X-ray photoelectron spectroscopy, *Applied Surface Science Advances* **5** (2021) 100112. https://doi.org/https://doi.org/10.1016/j.apsadv.2021.100112

[15] W. S. Hummers Jr., R. E. Offeman, Preparation of Graphitic Oxide, *Journal of the American Chemical Society* **80** (1958) 1339-1339. https://doi.org/10.1021/ja01539a017

[16] D. C. Marcano, D. V. Kosynkin, J. M. Berlin, A. Sinitskii, Z. Sun, A. Slesarev, L. B. Alemany, W. Lu, J. M. Tour, Improved Synthesis of Graphene Oxide, *ACS Nano* **4** (2010) 4806-4814. https://doi.org/10.1021/nn1006368

[17] S. Cheemalapati, S. Palanisamy, S.-M. Chen, Electrochemical Determination of Isoniazid at Electrochemically reduced graphene oxide modified Electrode, *International Journal of Electrochemical Science* **8** (2013) 3953-3962. https://doi.org/10.1016/S1452-3981(23)14444-0

[18] Y.-H. Chen, R. Kirankumar, C.-L. Kao, P.-Y. Chen, Electrodeposited Ag, Au, and AuAg nanoparticles on graphene oxide-modified screen-printed carbon electrodes for the voltammetric determination of free sulfide in alkaline solutions, *Electrochimica Acta* **205** (2016) 124-131. https://doi.org/10.1016/j.electacta.2016.04.111

[19] U. Koelle, A. Laguna, Electrochemistry of Au-complexes, *Inorganica Chimica Acta* **290** (1999) 44-50. https://doi.org/10.1016/S0020-1693(99)00112-7

[20] S. Y. Toh, K. S. Loh, S. K. Kamarudin, W. R. W. Daud, Graphene production via electrochemical reduction of graphene oxide: Synthesis and characterisation, *Chemical Engineering Journal* **251** (2014) 422-434. https://doi.org/10.1016/j.cej.2014.04.004

[21] Y. Xu, M. Gao, G. Zhang, X. Wang, J. Li, S. Wang, Y. Sang, Electrochemically reduced graphene oxide with enhanced electrocatalytic activity toward tetracycline detection, *Chinese Journal of Catalysis* **36** (2015) 1936-1942. https://doi.org/10.1016/S1872-2067(15)60956-1

[22] P. E. Rider, K. A. Gschneidner Jr., O.D. McMasters, Gold-rich rare-earth-gold solid solutions, *Transactions of the Metallurgical Society of AIME* **233** (1965) 1488-1496. https://www.osti.gov/biblio/4616986

[23] S. Z. Bas, Gold nanoparticle functionalized graphene oxide modified platinum electrode for hydrogen peroxide and glucose sensing, *Materials Letters* **150** (2015) 20-23. https://doi.org/10.1016/j.matlet.2015.02.130

[24] P. K. Sahoo, S. Sahoo, A. K. Satpati, D. Bahadur, Solvothermal synthesis of reduced graphene oxide/Au nanocomposite-modified electrode for the determination of inorganic mercury and electrochemical oxidation of toxic phenolic compounds, *Electrochimica Acta* **180** (2015) 1023-1032. https://doi.org/10.1016/j.electacta.2015.09.018

[25] S. Stankovich, D. A. Dikin, R. D. Piner, K. A. Kohlhaas, A. Kleinhammes, Y. Jia, Y. Wu, S. T. Nguyen, R. S. Ruoff, Synthesis of graphene-based nanosheets via chemical reduction of exfoliated graphite oxide, *Carbon* **45** (2007) 1558-1565. https://doi.org/10.1016/j.carbon.2007.02.034

[26] K. Ghanbari, A. Hajian, Electrochemical characterization of Au/ZnO/PPy/RGO nanocomposite and its application for simultaneous determination of ascorbic acid, epinephrine, and uric acid, *Journal of Electroanalytical Chemistry* **801** (2017) 466-479. https://doi.org/10.1016/j.jelechem.2017.07.024

[27] Y. Qin, J. Li, Y. Kong, X. Li, H. Xue, In Situ Synthesis of Photoreduced Au Nanoclusters Decorated-Graphene Hybrid as a High Efficient Electrocatalyst, *Journal of The Electrochemical Society* **161** (2014) H172. https://doi.org/10.1149/2.025404jes

[28] M. Turner, V. B. Golovko, O. P. Vaughan, P. Abdulkin, A. Berenguer-Murcia, M. S. Tikhov, B. F. Johnson, R. M. Lambert, Selective oxidation with dioxygen by gold nanoparticle catalysts derived from 55-atom clusters, *Nature* **454** (2008) 981-983. https://doi.org/10.1038/nature07194

[29] Z. Song, W. Li, F. Niu, Y. Xu, L. Niu, W. Yang, Y. Wang, J. Liu, A novel method to decorate Au clusters onto graphene via a mild co-reduction process for ultrahigh catalytic activity, *Journal of Materials Chemistry A* **5** (2017) 230-239. https://doi.org/10.1039/C6TA08284J

[30] J. Wang, *Analytical Electrochemistry*, John Wiley & Sons, USA, 2006. https://doi.org/10.1002/0471790303

[31] A. J. Bard, L. R. Faulkner, *Electrochemical methods: fundamentals and applications*, John Wiley & Sons, USA, 2001. ISBN 0-471-04372-9

[32] A. J. S. Ahammad, T. Islam, M. M. Hasan, M. N. I. Mozumder, R. Karim, N. Odhikari, P. R. Pal, S. Sarker, D. M. Kim, Reduced Graphene Oxide Screen-Printed FTO as Highly Sensitive Electrodes for Simultaneous Determination of Dopamine and Uric Acid, *Journal of The Electrochemical Society* **165** (2018) B174. https://doi.org/10.1149/2.0121805jes

[33] Y. Pang, Y. Zhang, X. Sun, H. Ding, T. Ma, X. Shen, Synergistical accumulation for electrochemical sensing of 1-hydroxypyrene on electroreduced graphene oxide electrode, *Talanta* **192** (2019) 387-394. https://doi.org/10.1016/j.talanta.2018.08.042

[34] E. Murugan, P. Arumugam, M. Kesava, A. Vinitha, Synthesis and characterization of graphene nanosheets for electrochemical quantification of chlorpheniramine maleate drugs using a

modified glassy carbon electrode, *Indian Journal of Chemical Technology* **29** (2022) 713-720. https://doi.org/10.56042/ijct.v29i6.67423

[35] S. I. Khan, R. V. Motghare, Electrochemical Determination of Chlorophenaramine Based on RTIL/CNT Composite Modified Glassy Carbon Electrode in Pharmaceutical Samples, *Journal of The Electrochemical Society* **166** (2019) B1202. https://doi.org/10.1149/2.0911913jes

[36] M. Amiri, M. Alimoradi, K. Nekoueian, A. Bezaatpour, Cobalt Flower-like Nanostructure as Modifier for Electrocatalytic Determination of Chloropheniramine, *Industrial & Engineering Chemistry Research* **51** (2012) 14384-14389. https://doi.org/10.1021/ie3016736

[37] A. S. Rajpurohit, A. K. Srivastava, Simultaneous electrochemical sensing of three prevalent anti-allergic drugs utilizing nanostructured manganese hexacyanoferrate/chitosan modified screen printed electrode, *Sensors and Actuators B* **294** (2019) 231-244. https://doi.org/10.1016/j.snb.2019.05.046

[38] D. E. Bayraktepe, Z. Yazan, Two-layered Au@Ag Bimetallic Nanocomposites-poly (L-Met) Platform for Highly Sensitive Chlorpheniramine Maleate Detection, *Electroanalysis* **34** (2022) 445-454. https://doi.org/10.1002/elan.202100422

[39] N. Shetti, D. Nayak, Electrochemical detection of chlorpheniramine maleate in the presence of an anionic surfactant and its analytical applications, *Canadian Journal of Chemistry* **95** (2017) 553-559. https://doi.org/10.1139/cjc-2016-0406

[40] P. Pinyou, V. Blay, J. Pansalee, S. Ramkrathok, T. Phetmuenwai, J. Jakmunee, K. Chansaenpak, S. Lisnund, Co-deposition of Graphene Oxide and Silver Nanoparticles for the Voltammetric Sensing of Chlorpheniramine, *Electrocatalysis* **14** (2023) 648-658. https://doi.org/10.1007/s12678-023-00826-x

[41] T. C. Pereira, N. R. Stradiotto, Electrochemical sensing of lactate by using an electrode modified with molecularly imprinted polymers, reduced graphene oxide and gold nanoparticles, *Microchimica Acta* **186** (2019) 764. https://doi.org/10.1007/s00604-019-3898-3

[42] S. D. Lamani, R. N. Hegde, A. P. Savanur, S. T. Nandibewoor, Voltammetric Determination of Chlorpheniramine Maleate Based on the Enhancement Effect of Sodium-dodecyl Sulfate at Carbon Paste Electrode, **23** (2011) 347-354. https://doi.org/10.1002/elan.201000369

[43] D. A. C. Brownson, C. E. Banks, *The Handbook of Graphene Electrochemistry,* Springer-Verlag London Ltd., 2014. https://doi.org/10.1007/978-1-4471-6428-9

[44] J. Soleymani, M. Hasanzadeh, N. Shadjou, M. Khoubnasab Jafari, J.V. Gharamaleki, M. Yadollahi, A. Jouyban, A new kinetic–mechanistic approach to elucidate electrooxidation of doxorubicin hydrochloride in unprocessed human fluids using magnetic graphene based nanocomposite modified glassy carbon electrode, *Materials Science and Engineering C* **61** (2016) 638-650. https://doi.org/10.1016/j.msec.2016.01.003

[45] M. A. Raj, S. A. John, Fabrication of Electrochemically Reduced Graphene Oxide Films on Glassy Carbon Electrode by Self-Assembly Method and Their Electrocatalytic Application, *The Journal of Physical Chemistry C* **117** (2013) 4326-4335. https://doi.org/10.1021/jp400066z

[46] W. Horwitz, R. Albert, Quality IssuesThe Concept of Uncertainty as Applied to Chemical Measurements, *Analyst* **122** (1997) 615-617. https://doi.org/10.1039/A703178E

[47] P. Konieczka, *Quality Assurance and Quality Control in the Analytical Chemical Laboratory*, CRC Press Taylor & Francis Group, 2018, https://doi.org/10.1201/9781315295015

[48] J. N. Miller, J. C. Miller, R. D. Miller, *Statistics and Chemometrics for Analytical Chemistry*, Pearson Education Limited, UK, 2018. https://api.pageplace.de/preview/DT0400.9781292186726_A36382216/preview-9781292186726_A36382216.pdf

[49] D. Eskiköy Bayraktepe, E. K. İnal, Z. Yazan, Preparation and characterization of a pencil graphite electrode modified with gold nanoparticles decorated poly (l-methionine) and its use in the simultaneous sensitive electrochemical analysis of ascorbic acid, acetaminophen,

chlorpheniramine maleate, and caffeine, *Microchemical Journal* **171** (2021) 106812. https://doi.org/10.1016/j.microc.2021.106812

[50] M. Perez-Ortiz, P. Pizzaro, A. Álvarez-Lueje, Carbon nanotubes–ionic liquid gel. characterization and application to pseudoephedrine and chlorpheniramine determination in pharmaceuticals, *Journal of the Chilean Chemical Society* **64** (2019) 4323-4331. https://doi.org/10.4067/s0717-97072019000104324

[51] Z. Pourghobadi, R. Pourghobadi, Electrochemical Behavior and Voltammetric Determination of Chlorpheniramine Maleate by Means of Multiwall Carbon Nanotubes-Modified Glassy Carbon Electrode, *International Journal of Electrochemical Science* **10** (2015) 7241-7250. https://doi.org/10.1016/S1452-3981(23)17345-7

[52] E. A. Khudaish, M. Al-Hinaai, S. Al-Harthy, K. Laxman, Electrochemical oxidation of chlorpheniramine at polytyramine film doped with ruthenium (II) complex: Measurement, kinetic and thermodynamic studies, *Electrochimica Acta* **135** (2014) 319-326. https://doi.org/10.1016/j.electacta.2014.05.029

[53] B. Magnusson, U. Örnemark, *Eurachem Guide: The Fitness for Purpose of Analytical Methods – A Laboratory Guide to Method Validation and Related Topics*, 2014. ISBN 978-91-87461-59-0

[54] AOAC International, *Appendix F: Guidelines for Standard Method Performance Requirements*, 2016, https://www.aoac.org/wp-content/uploads/2019/08/app_pdf

[55] Y. Liu, B. Zhu, M. Xue, Z. Jiang, X. Guo, Studies on the chiral separation of pheniramine and its enantioselective pharmacokinetics in rat plasma by HPLC-MS/MS, *Microchemical Journal* **156** (2020) 104989. https://doi.org/10.1016/j.microc.2020.104989

[56] P. Butmee, G. Tumcharern, G. Thouand, K. Kalcher, A. Samphao, An ultrasensitive immunosensor based on manganese dioxide-graphene nanoplatelets and core shell Fe_3O_4@Au nanoparticles for label-free detection of carcinoembryonic antigen, *Bioelectrochemistry* **132** (2020) 107452. https://doi.org/10.1016/j.bioelechem.2019.107452

[57] Ministry of Health, *Regulations on the list of prohibited substances used in the production and trading of health protection foods*, Viet Nam, 2021, https://thuvienphapluat.vn/van-ban/The-thao-Y-te/Thong-tu-10-2021-TT-BYT-Danh-muc-chat-cam-su-dung-san-xuat-thuc-pham-bao-ve-suc-khoe-481014.aspx

[58] Q. Hu, Y-I Cui, K. Wang, S. Ji, Detection of 16 anti-inflammatory and anti-histamine chemical drugs added illegally into traditional Chinese medicine and health food by liquid chromatography-ion trap mass spectrometry method, *Chinese Journal of Pharmaceutical Analysis* **12** (2008) 2065-2068. https://www.ingentaconnect.com/content/jpa/cjpa/2008/00000028/00000012/art00022

[59] J. Y. Kim, J. Y. Choi, C. Y. Yoon, S. Cho, W. S. Kim, J. A. Do, LC–MS/MS monitoring of 22 illegal antihistamine compounds in health food products from the Korean market, *Journal of the Korean Society for Applied Biological Chemistry* **58** (2015) 137-147. https://doi.org/10.1007/s13765-015-0004-3

[60] A. Nili-Ahmadabadi, Z. Borzouee, D. Ahmadimoghaddam, F. Firozian, D. Dastan, The occurrence of acetaminophen/codeine as an adulterant in herbal analgesic supplements in Hamadan, Iran: A pilot study, *Complementary Therapies in Medicine* **42** (2019) 223-225. https://doi.org/10.1016/j.ctim.2018.11.018